

Paranetric Down-Conversion Luminescence: A Fertile Ground in Quantum Optics

G. A. Barbosa

Departamento de Física - ICEx, Universidade Federal de Minas Gerais

C. P. 702, Belo Horizonte, 30161-970M.G., Brazil

e-mail : gbarbosa@fisica.ufmg.br

Received August 1, 1995

Research on parametric downconversion luminescence has been intensified recently providing remarkable tests of fundamental physics and revealing an appealing potentiality to applications that could not be developed with classical fields. This short review sketches the basics of the multi-mode theory for the phenomenon of down-conversion luminescence, discuss a few recent results and mentions some of the applications being envisaged.

Introduction

In spontaneous parametric downconversion luminescence (PDC), a nonlinear second order process, one photon from a pump laser at frequency ω_p – usually at U.V. frequencies – excites a nonlinear crystal non-resonantly, in a virtual process. The crystal decays within a very short time ($\Delta t \rightarrow 0$) of the excitation, due to this virtual character. The energy in the decay process can be converted into two simultaneous photons of energies ω_i and ω_s ¹. Due to energy and momentum conservation, $\hbar\omega_p = \hbar\omega_s + \hbar\omega_i$ and $\hbar\mathbf{k}_p = \hbar\mathbf{k}_s + \hbar\mathbf{k}_i$.

These conditions establish that no energy or momentum are taken by the crystal in the down-conversion process. However, the photon energies $\hbar\omega_s$ and $\hbar\omega_i$, and their respective momenta are not uniquely defined, the only condition being on their constant sum. Consequently, submitted to a stationary input of photons, the crystal produces a spectacular rainbow of colors as output. This rainbow can be easily seen with naked eyes at modest pump intensities.

At low pump intensities, at the instant of each photon excitation of the crystal, no signal or idler photon are present. The decaying processes can be considered as produced by random vacuum field fluctuations and, within this view, that rainbow is seen as a visual manifestation of "amplification of vacuum quantum noise". Although the pumping laser photons may be highly coherent, the down-converted photons do not

carry this coherence. The spontaneous decay, at random times, produces the randomness among phases of different photon pairs. The decay, for a given wavelength, has the characteristics of a chaotic or thermal-like source, with a Bose-Einstein photon probability distribution $p(n)$. Besides this chaotic character, an U.V. pump photon could have been converted to any conjugated pair, at different directions and random time instants.

The energy and momentum constraints, at the photon source, establish strong temporal and spatial correlation properties between the signal and idler photons. After being generated, strongly correlated, the propagating photon pair will carry informations on the correlations established at the source. These correlations, present at the far-field radiation, can be explored in many ways. Non-local properties can be used to check hypothesis on the non-existence of elements of the physical reality, in applications in the communication field, in the construction of quantum interferometers and many other studies and applications, including low noise measurements with quantum microscopes, polarimeters, low noise spectroscopy, etc.

This review is planned as follows: The first section, entitled *Theoretical elements of the parametric down-conversion luminescence*, gives the basic elements of the theory and intends to give a working knowledge to the reader.

¹The conventional indexes *s* and *i* stands for *signal* and *idler*, respectively. For historical reasons, the name *signal* is applied to the photon of lower energy in the pair but, indeed, either photon can be arbitrarily called signal or idler.

The second section, *Reflections of a single-photon in a cavity* shows a simple application of coincidence measurements on a pair of down-converted photons. The third one, *Induced coherence without stimulated emission*, exposes a new phenomenon discovered by Manciel and co-authors where tests of coherence concepts can be broadly explored. This phenomenon can be seen as a new type of a double-slit Young experiment, where slits were substituted by active crystals. The analogous interference to the Young experiment is here produced by light emitted from these crystals. In a sense, it opens novel study possibilities on the Young-slit experiment, so fundamental to the analysis of classical and quantum interference phenomena. Aspects that influence the fringes visibility can be studied including basic aspects of light-matter interaction.

The fourth section, *Visibility control*, explores ways to change the visibility in the "induced coherence without stimulated emission" through changes in the idler beam connection path. Ways of changing the visibility are explored including a Berry's phase experiment and a proposed experimental configuration to increase the visibility of fringes produced in experiments with down-converted light.

The fifth section, *Forced indistinguishability in "induced coherence without stimulated emission"*, shows a proposal to maximize the visibility degree and the experimental difficulties to achieve high values of the visibility. The sixth section, *Young fringes and non-localized control of visibility*, explores a few ways to a non-local control of visibility of the interference fringe patterns and its connection to the "quantum-image" concept. The section *"Beam-splitters, cavities and some applications"* introduces the basic "two-port" formalism to deal with beam splitters and cavities and indicates, as an application, the idea of an *active* cavity designed to manipulate the photon statistics generated in the down-conversion process.

The final section, *Conclusions*, emphasizes the richness of this phenomenon, and indicates applications in the communication field, low noise measurements with

squeezed fields and the construction of widely tunable sources of non-classical light.

I. Theoretical elements of the parametric down-conversion luminescence

1.1 Multi-mode and single-mode theories

The experimental facts on the *parametric down-conversion luminescence* (PDC) have to be explained including the simultaneous detection of conjugated photon pairs. Theories taking into account temporal detection of pulses, as in coincidence measurements, are multi-mode theories, due to the necessity of constructing localized wave-packets. Single mode theories would predict an uniform time detection probability to find photons in the field - not the localized conjugated photons detected in coincidence measurements. Mandel and co-authors^[1] developed the basic multi-mode theory presented in this section which has been applied successfully by several groups². Of course, the interaction mechanism follows basic ideas formerly developed by Louisell and others^[3].

The most common types of PDC are called types I and II, where in type I the converted beams have polarizations normal to the polarization of the pump laser and in type II one beam has polarization normal to the pump beam and the other has polarization parallel to it³. These solutions appear naturally as solutions to Fresnel's equations^[5].

Fig. 1 shows the basic setup for the detection of the signal-idler conjugated pair. Pinholes are used to define directions as well as to help in the elimination of undesired light backgrounds. Pinholes are also spatial wavelength filters for the rainbow light, according to the relationships between wavevectors and down-conversion angles. Besides pinholes, interference filters ($\Delta\lambda \sim 10, 100 \text{ \AA}$) are commonly used to define the collected wavelength interval.

²Comments on a non-equivalence between multi-mode theories have been made by some authors. See, for example Ref. [2].

³A third type may occur whenever the birefringence is very high, and it is known as type III. While a bit artificial in its definition, with the convention $\omega_1 < \omega_2 < \omega_3$, these solutions^[4] are arranged according the following table where o and e specifies ordinary and extraordinary polarizations, respectively. ω_1 and ω_2 are signal or idler frequencies and ω_3 is the laser frequency.

Type	I	II	III
------	---	----	-----

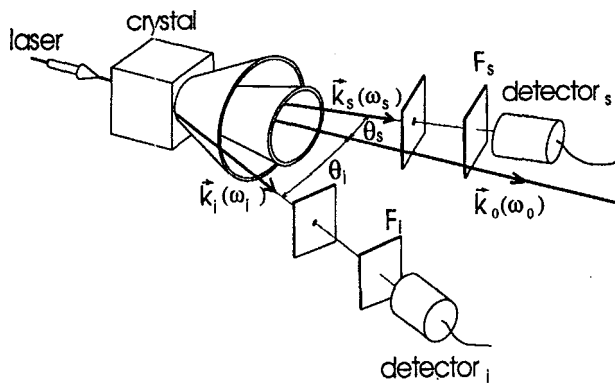


Figure 1. Basic setup for parametric down-conversion luminescence: A laser of frequency ω_p and wavevector \mathbf{k}_p excites a nonlinear crystal. \mathbf{k}_s and \mathbf{k}_i are the conjugated wavevectors "signal" and "idler", such that $\mathbf{k}_p = \mathbf{k}_s + \mathbf{k}_i$ and $\omega_p = \omega_s + \omega_i$. \mathbf{k}_s and \mathbf{k}_i are located in "cones" of frequency ω_s and ω_i . Different conjugated pairs can be chosen within these cones as long as energy and momentum conservation conditions are obeyed. The conjugated beams trajectories are marked by pinholes. Interference filters F_s and F_i are placed just before the detectors. θ_s and θ_i are the angles between each conjugated beam and the pump beam.

How narrow could one define the collected wavelength intervals? In principle, no optical filter can be single-mode without violating *causality*.^[6] However, bandwidths can be arbitrarily small without violating the limit imposed by causality. Although very narrow filtering could then be done, the signal to noise ratios actually establish the practical limits in filtering.

Even when dealing with very low photon counting rates, say, one or less than one photon per coherence time, the photon energy $\hbar\omega$ cannot be known better than the precision given by the frequency bandwidth $\Delta\omega$ of the narrowest filter utilized. Consequently, even

with one photon present a single photon wavepacket has to be associated to it.

The wavepacket treatment is necessary to deal with simultaneous or coincidence measurements because slight delays imposed between the two detectors may lead to no coincidence between conjugated photons. On the other hand, although single mode theories give some basic results and insights into the PDC, they predict a uniform probability to find a photon in either conjugated beam and, in this way, coincidence rates just show random coincidences, not adequate to experimental comparisons whenever time delays are involved.

1.2 Hamiltonian weak nonlinear interaction

Electric fields in the neighborhood of molecules or atoms can be quite intense, of order of a few volts per Å, or $\sim 10^8$ V/m. A pulsed laser may reach intense fields (a light power of 1 MW/mm² gives $\sim 3 \times 10^7$ V/m) and can induce appreciable nonlinear effects. In this regime, molecules are deformed, say, in a reversible way⁴, beyond Hooke's limit, or linear limit.

CW lasers, of lower power ($P = 100$ mW in 1mm² would give $\sim 10^0$ V/m), lead to weak nonlinear effects and, consequently, first order terms in a perturbation theory will suffice to take care of these effects. In this case, the downconversion rate is also low, say an average number of photons ($n \ll 1$ per coherence time). This is certainly a proper domain for a quantum treatment.

In this range of weak fields the nonlinear medium polarization can be safely written^[7] as

$$\begin{aligned}
 \mathbf{P} &= \int_0^\infty \chi^{(1)}(t') \mathbf{E}(\mathbf{r}, t - t') dt' \\
 &+ \int_0^\infty \int_0^\infty \chi^{(2)}(t', t'') \mathbf{E}(\mathbf{r}, t - t') \mathbf{E}(\mathbf{r}, t - t'') dt' dt''
 \end{aligned}
 \tag{1}$$

⁴ Irreversible deformations are associated with crystal damage, a non negligible factor in several experiments.

where $\chi^{(1)}$ and $\chi^{(2)}$ are the first and second order electrical susceptibilities. For crystals without inversion symmetry centers⁵, $\chi^{(2)} \neq 0$.

The time dependence in the integrals show that retarded effects could contribute to the polarization and a simple dependence on the position was written implying local responses as a simplification.

Other simplifications are going to be considered, namely, low absorption and low dispersion at the involved wavelengths. The low dispersion means that the refractive index should not show appreciable variations around these wavelengths.

Classically, the electromagnetic energy density in matter is^[7]

$$u = \frac{1}{2}(\mathbf{D} \cdot \mathbf{E} + \mathbf{B} \cdot \mathbf{H}), \quad (2)$$

where \mathbf{D} is the electric displacement vector and \mathbf{B} is the magnetic field.

Our choice is to write the main term, the *linear* one, of the electromagnetic energy explicitly in the Hamiltonian,

$$\hat{\mathcal{H}}_0 = \frac{1}{2} \int_{V_I} (\hat{\mathbf{D}} \cdot \hat{\mathbf{E}} + \hat{\mathbf{B}} \cdot \hat{\mathbf{H}}) d\mathbf{r}, \quad (3)$$

where V_I is the interaction volume. Hats over a generic symbol designate quantum operators.

The small nonlinear term will be written as a perturbation $\hat{\mathcal{V}}$ added to $\hat{\mathcal{H}}_0$:

$$\hat{\mathcal{V}} = \frac{1}{2} \int_{V_I} \hat{\mathbf{E}} \cdot \hat{\mathbf{P}}^{NL} d\mathbf{r} = \frac{1}{2} \int_{V_I} \hat{\mathbf{E}}_i(\mathbf{r}, t) \int_0^\infty \int_0^\infty \chi^{(2)}_{ijk}(t', t'') \hat{\mathbf{E}}_j(\mathbf{r}, t - t') \hat{\mathbf{E}}_k(\mathbf{r}, t - t'') dt' dt'' d\mathbf{r} \quad (4)$$

To quantize the electric fields, the classical amplitudes a will be substituted by operators \hat{a} and the quantized field will be written as

$$\hat{\mathbf{E}}(\mathbf{r}, t) = \hat{\mathbf{E}}^-(\mathbf{r}, t) + \hat{\mathbf{E}}^+(\mathbf{r}, t), \quad (5)$$

where

$$\hat{\mathbf{E}}^+(\mathbf{r}, t) = [\hat{\mathbf{E}}^-(\mathbf{r}, t)]^\dagger = \frac{1}{\sqrt{V}} \sum_{\mathbf{k}, s} \mathbf{e}_{\mathbf{k}, s} l(\omega) \hat{a}_{\mathbf{k}, s} e^{i(\mathbf{k} \cdot \mathbf{r} - \omega t)}, \quad (6)$$

and $\mathbf{e}_{\mathbf{k}, s}$ is the unit vector indicating mode polarization, while $\hat{a}_{\mathbf{k}, s}$ is the annihilation operator and

$$l(\omega) = i \left[\frac{\hbar \omega(\mathbf{k}, s)}{2 \epsilon_0 n^2(\mathbf{k}, s)} \right]^{1/2}. \quad (7)$$

The quantization volume V appearing in the electric

field, Eq. (6), is written $V = AL$, where A is the mode cross section and L its coherence length, that is to say, $L = \frac{c}{\delta \nu} = \frac{2\pi c}{\delta \omega}$.

Substituting the electric field, Eq. (6), in $\hat{\mathcal{H}}_0$ and in the nonlinear part of the energy, written as $\hat{\mathcal{V}}$, it follows⁶ that^[1]

$$\hat{\mathcal{H}} = \hat{\mathcal{H}}_0 + \hat{\mathcal{V}}, \quad (8)$$

⁵The polar character of the polarization implies that, under inversion upon a symmetry center, \mathbf{P} would be transformed to $-\mathbf{P}$. The second-order polarizability, depending on E^2 , implies that $\chi^{(2)} = 0$ in these crystals.

⁶A simplification of a uniform transverse cross-section illumination due to the pump laser is usually assumed. A more realistic dependence could be used, such as a gaussian profile for the laser beam.

with

$$\begin{aligned} \hat{\mathcal{H}}_0 &= \sum_{\mathbf{k}_j, s_j} \hbar \omega_j a_{\mathbf{k}_j, s_j}^\dagger a_{\mathbf{k}_j, s_j}, \\ &\text{where } j = 1, 2, 3 \text{ and} \\ \hat{\mathcal{V}} &= \frac{1}{V^{3/2}} \sum_{\mathbf{k}_1, s_1} \sum_{\mathbf{k}_2, s_2} \sum_{\mathbf{k}_3, s_3} l^*(\omega_1) l^*(\omega_2) l(\omega_3) \hat{a}_{\mathbf{k}_1, s_1}^\dagger \hat{a}_{\mathbf{k}_2, s_2}^\dagger \hat{a}_{\mathbf{k}_3, s_3} \times \\ &\quad \times e^{i(\omega_1 + \omega_2 - \omega_3)t} [\tilde{\chi}_{ijk}^{(2)}(\mathbf{e}_{\mathbf{k}_3, s_3})_i (\mathbf{e}_{\mathbf{k}_1, s_1})_j^* (\mathbf{e}_{\mathbf{k}_2, s_2})_k^*] \times \\ &\quad \times \int_{V_I} e^{-i(\mathbf{k}_1 + \mathbf{k}_2 - \mathbf{k}_3) \cdot \mathbf{r}} d\mathbf{r} + \text{H.c.}, \end{aligned} \tag{9}$$

where H.c. indicates the Hermitian conjugated of the first term and

$$\tilde{\chi}_{ijk}^{(2)}(\omega = \omega' + \omega'') \equiv \int_0^\infty \int_0^\infty \chi_{ijk}^{(2)}(t', t'') e^{i(\omega' t' + \omega'' t'')} dt' dt''. \tag{10}$$

Note that the indexes 1, 2 and 3 are denoting signal, idler and pump laser, respectively; sometimes along the paper the indexes *s*, *i*, and *p* will be used substituting 1, 2 and 3.

1.3 Single-mode Hamiltonian and equations of motion

A finite size crystal or, more precisely, a finite illuminated region always imply in diffraction of the generated luminescence. The term $\int_{V_I} e^{-i(\mathbf{k}_1 + \mathbf{k}_2 - \mathbf{k}_3) \cdot \mathbf{r}} d\mathbf{r}$ in $\hat{\mathcal{V}}$ gives, in the limit of an infinite illuminated region, a Dirac delta⁷ forcing that $\mathbf{k}_1 + \mathbf{k}_2 = \mathbf{k}_3$. In this way, the divergence of the conjugated beams are eliminated. While this is a enormous simplification, it is not realistic for the size of crystals one normally deals with. Despite this, single-mode theories allow several studies and its importance cannot be denied. A single mode approximation can be achieved neglecting divergences, and imply the utilization of idealized monochromatic

filters. A simple form for $\hat{\mathcal{V}}$ is then obtained through the simplification of the sums on the wavevectors {*k*}.

Usually some absorption is present at the pump laser wavelength but if this absorption can be neglected, the annihilation operator $\hat{a}_{\mathbf{k}_3, s_3}$ for the pump laser photons can be substituted by a classical amplitude *v*. The down-conversion process itself will drain energy from the pump laser beam but this loss is negligible compared with the pump beam energy within the same time span.

With these simplifications this single mode Hamiltonian will be indicated by $\hat{\mathcal{H}}_m$. The interaction Hamiltonian,

$$\hat{\mathcal{H}}_I = \exp\left(i \frac{\hat{\mathcal{H}}_0 t}{\hbar}\right) \hat{\mathcal{H}}_m \exp\left(-i \frac{\hat{\mathcal{H}}_0 t}{\hbar}\right),$$

is

$$\hat{\mathcal{H}}_I = \hbar \omega_a \hat{a}^\dagger \hat{a} + \hbar \omega_b \hat{b}^\dagger \hat{b} + i \hbar g v (e^{-i\omega_p t} \hat{a}^\dagger \hat{b}^\dagger - e^{i\omega_p t} \hat{b} \hat{a}). \tag{11}$$

where $\hat{a}_1 \rightarrow \hat{a}$ and $\hat{a}_2 \rightarrow \hat{b}$ simplifies the notation and *g* includes parameters of the Hamiltonian $\hat{\mathcal{H}}$, Eq.(8).

Equations of motion for the operators \hat{a} , \hat{b}^\dagger and their

adjoints can be obtained from the Heisenberg equations of motion

$$i \hbar \frac{d}{dt} \hat{a} = [\hat{a}, \hat{\mathcal{H}}_I], \tag{12}$$

⁷ $\int_{V \rightarrow \infty} e^{-i(\mathbf{k}_1 + \mathbf{k}_2 - \mathbf{k}_3) \cdot \mathbf{r}} d\mathbf{r} \equiv \delta(\mathbf{k}_1 + \mathbf{k}_2 - \mathbf{k}_3)$

and similar equations for the remaining operators.

From the Hamiltonian $\hat{\mathcal{H}}_I$ one obtains

$$\begin{aligned} \frac{d}{dt}\hat{a}(t) &= -i\omega_a \hat{a}(t) + gve^{-i\omega_p t} \hat{b}^\dagger(t) \\ \frac{d}{dt}\hat{b}^\dagger(t) &= i\omega_b \hat{b}^\dagger(t) + gve^{i\omega_p t} \hat{a}(t), \end{aligned} \quad (13)$$

and their adjoints. The laser frequency is written as ω_0 , with $\omega_0 = \omega_a + \omega_b$. A Laplace transform of these equations gives

$$\begin{aligned} (s + i\omega_a)\hat{a}(s) - gv\hat{b}^\dagger(s + i\omega_p) &= \hat{a}(0) \\ -gv\hat{a}(s) + (s + i\omega_b)\hat{b}^\dagger(s + i\omega_p) &= \hat{b}^\dagger(0), \end{aligned} \quad (14)$$

and their inverse transform give

$$\hat{a}(t) = e^{-i\omega_a t} [\cosh(g|v|t)\hat{a}(0) + \sinh(g|v|t)\hat{b}^\dagger(0)]$$

$$\hat{b}^\dagger(t) = e^{i\omega_b t} [\cosh(g|v|t)\hat{b}^\dagger(0) + \sinh(g|v|t)\hat{a}(0)] \quad (15)$$

One should note that no energy loss is included in these equations. The simplicity of these solutions allows straightforward calculations in several cases.

1.4 PDC - a squeezed light field

A special character of this field can be seen through the quadrature components of the electric field for the signal and idler beams, written (see Ref. [8] as an example) as

$$\hat{X}_1(t) \equiv \frac{1}{\sqrt{2}} [\hat{a}(t)e^{i\omega t} + \hat{a}^\dagger(t)e^{-i\omega t}], \text{ and } \hat{X}_2(t) \equiv \frac{2}{\sqrt{2}} [\hat{a}(t)e^{i\omega t} - \hat{a}^\dagger(t)e^{-i\omega t}]. \quad (16)$$

Substituting Eqs. (15) and their adjoint in these equations result in

$$\hat{X}_1(t) = e^{g|v|t}\hat{X}_1(0) \text{ and } \hat{X}_2(t) = e^{-g|v|t}\hat{X}_2(0), \quad (17)$$

and similar equations for the \hat{b} components.

These equations show that this field has a squeezed quadrature component^[8], a signature of a nonclassical field. In principle, each quadrature component can be explored by homodyne measurements^[9], taking into account the difference between counts from two detectors receiving a superposition of the downconverted and

laser light.

Quantum correlations between signal and idler can also be detected by direct subtraction of pulses between the idler and signal detectors^[10].

1.5 Non-locality of solutions

Another interesting aspect of this field may be obtained by introduction of a linear combination of operators to show some characteristics of the solutions in some special cases of our Hamiltonian $\hat{\mathcal{H}}_I$, Eq. (11). For example, the combination

$$\hat{c}_\pm = \frac{\hat{a} \pm \hat{b}}{\sqrt{2}}, \quad (18)$$

gives a matrix form for the symmetrized Hamiltonian

$$\hat{\mathcal{H}}_I = \begin{pmatrix} \hat{c}_+^\dagger & \hat{c}_+ & \hat{c}_-^\dagger & \hat{c}_- \end{pmatrix} \begin{pmatrix} \Delta^+ & igve^{-i\omega_p t} & \Delta^- & 0 \\ -igve^{i\omega_p t} & \Delta^+ & 0 & \Delta^- \\ \Delta^- & 0 & \Delta^+ & -igve^{-i\omega_p t} \\ 0 & \Delta^- & igve^{i\omega_p t} & \Delta^+ \end{pmatrix} \begin{pmatrix} \hat{c}_+ \\ \hat{c}_+^\dagger \\ \hat{c}_- \\ \hat{c}_-^\dagger \end{pmatrix},$$

where

$$\Delta^\pm = \frac{(\omega_a \pm \omega_b)}{4}.$$

As a simple case, one can look at the degenerated case $\omega_a = \omega_b$ or $\Delta^- = 0$. The Hamiltonian is decoupled in two blocks, indicating the existence of eigenvectors or eigenfunctions involving either \hat{c}_+ or \hat{c}_- , independently:

$$\hat{H}_I = (\hat{c}_+^\dagger \hat{c}_+ \hat{c}_-^\dagger \hat{c}_-)^\dagger \begin{pmatrix} \frac{\omega_a}{2} & igve^{-i\omega_p t} & 0 & 0 \\ -igve^{i\omega_p t} & \frac{\omega_a}{2} & 0 & 0 \\ 0 & 0 & \frac{\omega_a}{2} & -igve^{-i\omega_p t} \\ 0 & 0 & igve^{i\omega_p t} & \frac{\omega_a}{2} \end{pmatrix} \begin{pmatrix} \hat{c}_+ \\ \hat{c}_+^\dagger \\ \hat{c}_- \\ \hat{c}_-^\dagger \end{pmatrix}.$$

Solutions with \hat{c}_+ or \hat{c}_- refer to signal and idler beam together: that, after being generated, may propagate in two distinct regions of space. These solutions carry information on the entanglement occurred at the source, in the sense that any expected value brings the information non-locally, because this information is contained in the wavefunction predicting those values. Consequently, if one injects the signal and idler beams, for example, into separated optical fibers or optical guides, the information on the original entanglement will be carried non-locally along the whole fiber length.

Several applications in communication theory have been proposed based on this non-locality^[11]. Studies on the *non-existence* of certain "elements of the physical reality" have also profited of these peculiar conjugated light beams⁸.

1.6 Wavefunction in the number basis

The evolution of states given by the single-mode Hamiltonian \hat{H}_m can be written, in the interaction representation, by $|t\rangle_I$, a solution of the equation of motion

$$i\hbar \frac{\partial}{\partial t} |t\rangle_I = \hat{V}_I |t\rangle_I, \tag{19}$$

where $\hat{V}_I = \hbar(G \hat{a}^\dagger \hat{b}^\dagger + c.H.)$, and G includes parameters of the Hamiltonian given by Eq. (8). Given the wavefunction in $t = 0$, the wavefunction in $t = t_{int}$ is

$$|t_{int}\rangle_I \equiv |\zeta\rangle \simeq \exp(-i \frac{\hat{V}_I t_{int}}{\hbar}) |0, 0\rangle = e^{\zeta \hat{a}^\dagger \hat{b}^\dagger - \zeta^* \hat{a} \hat{b}} |0, 0\rangle, \tag{20}$$

where $\zeta = -iGt_{int}$ and the ket $|n_s = Q n_i = 0\rangle$ represents the initial state in the number basis. t_{int} defines the interaction time between the laser photons and the crystal, from $t = 0$ to $t = t_{int}$ or, equivalently, from $t - t_{int}$ to t .

The parametric down conversion occurs within a very short time interval after the crystal excitation by the pump laser. However, these time intervals are at random, characteristic of spontaneous emissions. This implies that at the excitation instant, no signal or idler photons are present. In other terms, the decaying process is said to occur from the vacuum. In a continuous (CW) operation, these processes will be continually repeated⁹.

Applying the evolution operator $e^{\zeta \hat{a}^\dagger \hat{b}^\dagger - \zeta^* \hat{a} \hat{b}}$ to $|0, 0\rangle$ one obtains^[14]

$$|\zeta\rangle = (\text{sech}|\zeta|) \sum_{n=0}^{\infty} \left(\frac{\zeta}{|\zeta|} \tanh|\zeta| \right)^n |n, n\rangle. \tag{21}$$

1.7 Photon statistics; mixtures

With this wavefunction, Eq. (21), one could calculate, for example, the probability to obtain n signal photons and n idler photons in the down-conversion process as

$$p(n, n) \text{ r } p(n) = |\langle n, n | \zeta \rangle|^2 = (\text{sech}|\zeta|)^2 (\tanh|\zeta|)^{2n} = \frac{(\sinh^2 |\zeta|)^n}{(1 + \sinh^2 |\zeta|)^{n+1}}. \tag{22}$$

⁸By *non-existence* of "elements of the physical reality" it is understood that only when the *measurement* operation is performed a certain quantity is specified. No physical meaning being assigned, say, to a photon polarization or spin components *before* the *measurement* is done [12]. Classical physics relies on the assumption of a physical reality independent of any measurement performed, a position opposite to the one taken by quantum mechanics. See Ref. [13] on existent loop holes in experiments with cascade sources and two-photon experiments aimed to test quantum-mechanics.

⁹The downconverted power at frequency ω is $P_d = \langle n \rangle \frac{\hbar\omega}{\tau_c}$, where $\langle n \rangle$ is the average number of photons within a coherence time τ_c . $P_d \sim 10^{-5}$ W for $\langle n \rangle \sim 1$ and $\tau_c \sim 10^{-14}$ s. With a crystal conversion efficiency of $|\eta|^2 \sim 10^{-10}$, this value of P_d would be obtained with a pump power of $P_l = \frac{P_d}{|\eta|^2} \sim 10^5$ W. CW lasers are well below this value and, consequently, $\langle n \rangle \ll 1$ within a coherence time. This justifies the assumption of no signal and idler photons present at the excitation times.

This statistical distribution probability is a Bose-Einstein distribution for photon emission with random phases, similar to a thermal emission. To make this more apparent, the average number of photons (n) can be calculated within a coherence time¹¹:

$$\langle n \rangle = \sinh^2 |\zeta|. \quad (26)$$

resulting in the traditional form of the Bose-Einstein distribution

$$p(n) = \frac{\langle n \rangle^n}{(1 + \langle n \rangle)^{n+1}}. \quad (27)$$

The spontaneous down-conversion shows a Bose-Einstein statistical distribution for photon counting; however, some other experimental arrangements may reveal different distributions. For example, through alignment of an auxiliary laser along the idler path (or signal path) and with identical wavelength as the idler (or signal) one, idler (or signal) decay will be stimulated by the laser field. As the energy conservation is kept through signal and idler photons, the conjugated signal (or idler) beam will be equally stimulated. One could ask about the statistical characteristics of the emerging signal and idler photons^[15] and its dependence on the intensity of the auxiliary laser beam.

The wavefunction is calculated as before, from

$$|t\rangle \equiv |\zeta\rangle = \exp\left(-i\frac{\hat{V}_I t}{\hbar}\right) |t=0\rangle = e^{\zeta\hat{a}^\dagger\hat{b}^\dagger - \zeta^*\hat{a}\hat{b}} |t=0\rangle. \quad (28)$$

The difference now is that the initial state, in $t=0$, is $|0, v\rangle = |0\rangle|v\rangle$, where v represents the coherent amplitude of the auxiliary laser beam. The coherent state^[16]

(v), defined by $\hat{b}|v\rangle = v|v\rangle$, is

$$|v\rangle = e^{-\frac{|v|^2}{2}} \sum_{n=0}^{\infty} \frac{v^n}{\sqrt{n!}} |n\rangle. \quad (29)$$

For a strong auxiliary laser, and $|v|^2 \gg 1$, the approximation $\hat{b} \rightarrow v$ can be safely used and the operator $\exp(\zeta\hat{a}^\dagger\hat{b}^\dagger - \zeta^*\hat{a}\hat{b})$ is then approximated by $\exp(\delta\hat{a}^\dagger - S^*\hat{a})$, where $\delta = \zeta v^*$.

Baker-Hausdorff's lemma¹¹ [18], applied to this operator gives

$$e^{\delta\hat{a}^\dagger - S^*\hat{a}} = e^{\delta\hat{a}^\dagger} e^{-S^*\hat{a}} e^{-\frac{|S|^2}{2}}. \quad (30)$$

A simple result is then achieved

$$\begin{aligned} |t\rangle &= e^{-\frac{|S|^2}{2}} e^{\delta\hat{a}^\dagger} |0\rangle|v\rangle \\ &= \left(e^{-\frac{|S|^2}{2}} \sum_{n=0}^{\infty} \frac{(\delta\hat{a}^\dagger)^n}{n!} |0\rangle \right) |v\rangle \\ &= |\delta\rangle|v\rangle = |\zeta v^*\rangle|v\rangle, \end{aligned} \quad (31)$$

giving the product of two coherent states¹² and, consequently, the Poissonian statistics associated with these states. In the case of an arbitrary amplitude for the auxiliary laser beam, the problem is more complex, involving the classical problem of ordering the photon operators to achieve easier calculation forms. Of course, series expansion of the operator $\exp(\zeta\hat{a}^\dagger\hat{b}^\dagger - \zeta^*\hat{a}\hat{b})$ can be always done up to any desired practical order.

$p(n, n)$ can be also found from wavefunctions in closed solution given in recurrence form. The following recurrence^[17] is an example of this approach applied to the case $|\zeta\rangle = \exp(\zeta\hat{a}^\dagger\hat{b}^\dagger - \zeta^*\hat{a}\hat{b}) |0\rangle|v\rangle$ (The reader may be challenged to write this result in terms of known functions and to obtain the resulting photon distribution probability!):

¹⁰

$$\langle n \rangle = \sum_{n=0}^{\infty} n p(n) \equiv \frac{1}{1+W} \sum_{n=0}^{\infty} n \left(\frac{W}{1+W} \right)^n, \quad (23)$$

where $W = \sinh^2 |\zeta|$. The above series, in the right hand side, has the form

$$S(y) = \sum_{n=0}^{\infty} n y^n = y \frac{d}{dy} \sum_{n=0}^{\infty} y^n = y \frac{d}{dy} \left(\frac{1}{1-y} \right), \quad (24)$$

$$\langle n \rangle = \sinh^2 |\zeta|. \quad (25)$$

¹¹If operators A e B have the commutator C , $[A, B] = C$, and if A and B commute with C , then $e^{A+B} = e^A e^B e^{-C/2}$.

¹²The resulting photon statistics for a coherent state $|v\rangle$ is given by the magnitude squared of $\langle n|v\rangle$, or, $p(n) \equiv |\langle n|v\rangle|^2 = e^{-|v|^2} |v|^{2n} / n!$, that is a Poisson distribution for the number of photons n and average photon number $\langle n \rangle = |v|^2$.

$$|\zeta\rangle = e^{-\frac{1}{2}|v|^2} \sum_{n=0}^{\infty} \sum_{m=0}^{\infty} \sum_{k=0}^{\infty} \frac{(-|\zeta|^2)^k}{(n+2k)!} f_{nk}^m \frac{v^m \zeta^n}{m!} \hat{a}^{\dagger n+m} \hat{b}^{\dagger n} |0,0\rangle, \tag{32}$$

where

$$f_{n0}^m = 1, \text{ and } f_{0k}^m = (n+1)f_{1k-1} \text{ and } f_{nk}^m = f_{n-1k}^m + (n+1)(m+n+1)f_{n+1k-1}^m \tag{33}$$

The photon statistics associated with this general case is more complicated but it reduces to the Poisson case for $|v| \gg 1$ and to the Bose-Einstein case for $v \rightarrow 0$. Measurements have not yet been done to verify these predictions. Anyway, this is a very difficult experimental problem due to the necessity of establishing a narrow bandwidth such that the coherence time of the wavepackets is long enough to be accessible by conventional electronics - $p(n)$ measurements have to be performed within sampling times shorter than the coherence times. A further complication is that several modes may be present, depending on the geometry used, and the statistics tend to become Poissonian due to the independence of their phases.

1.8 Multi-mode wavefunction

Multi-mode solutions are a necessity for many studies including coincidence measurements where wavepackets of finite size have to be defined. The time dependent Hamiltonian, Eq. (8), has a series solution for the wavefunction^[18,19]

$$|\psi(t)\rangle \equiv |t\rangle = \left[1 + \frac{1}{i\hbar} \int_{t-t_{int}}^t \hat{V}(\tau) d\tau + \dots \right] |0,0\rangle. \tag{34}$$

Each term in this expansion can be calculated in a straightforward manner although this process becomes quite tedious after the first terms. However, the first

term to be calculated is the dominant one whenever the pump beam is weak. Simple integrals are used in the development of this expression as, for example, (see Eq.(9)):

$$\begin{aligned} \int_{V_{illum.}} e^{i(\mathbf{k}_3 - \mathbf{k}_2 + \mathbf{k}_1) \cdot \mathbf{r}} d\mathbf{r} &\equiv \int_{V_{illum.}} e^{i(\Delta\mathbf{k}) \cdot \mathbf{r}} d\mathbf{r} \\ &= \int_{-l_1}^{l_1} dx' \int_{-l_2}^{l_2} dy' \int_{-l_3}^{l_3} dz' e^{i\Delta\mathbf{k} \cdot \mathbf{r}'} e^{i\Delta\mathbf{k} \cdot \mathbf{r}_0} \\ &= \prod_{m=1}^3 \left[\frac{\sin\left(\frac{\Delta k_m l_m}{2}\right)}{\left(\frac{\Delta k_m}{2}\right)} \right] e^{i\Delta\mathbf{k} \cdot \mathbf{r}_0}, \end{aligned} \tag{35}$$

where \mathbf{r}_0 is the origin of coordinates, that can be taken as $\mathbf{r}_0 = 0$; l_j indicate the sizes of illuminated region in the three orthogonal directions. This function shows that an increase in the size of the illuminated region gives a better definition of the downconverted light wavevector or, in a rough picture, the cone angular thickness, or divergence, in Fig. 1 is decreased.

Another integral occurring in the development of the wavefunction is

$$\int_{t-t_{int}}^t e^{i(\omega_1 + \omega_2 - \omega_3)t'} dt' = e^{i\Omega t} e^{-i\Omega \frac{t_{int}}{2}} \frac{\sin\left(\frac{\Omega}{2} t_{int}\right)}{\left(\frac{\Omega}{2}\right)}, \tag{36}$$

where $\Omega = \omega_1 + \omega_2 - \omega_3$. The finite integration time t_{int} shows that the Ω values are within $\Omega \sim \pi/t_{int}$.

With these integrals the calculation of $|t\rangle$ leads directly to

$$\begin{aligned} |t\rangle &= |0,0\rangle + \\ &+ \eta \frac{(\delta\omega)}{\sqrt{2\pi}} \sum_{\omega_1} \sum_{\omega_2} \sum_{\omega_3} e^{i\Omega(t - \frac{t_{int}}{2})} \phi(\omega_1, \omega_2; \omega_3) \frac{\sin\left(\frac{\Omega}{2} t_{int}\right)}{\left(\frac{\Omega}{2}\right)} \times \\ &\times v(\omega_3) |1_{\omega_1}\rangle |1_{\omega_2}\rangle + \dots \end{aligned} \tag{37}$$

This wavefunction, explicitly developed up to first order terms in number of photons, represents the process of down-conversion luminescence and contains the basic ingredients to the prediction and interpretation of a quite large number of effects.

The substitution $\sum_{\mathbf{k}(\omega)} \rightarrow \sum_{\omega}$ in the development

of the wavefunction was made implying the simplification of a mutual correspondence $\mathbf{k}(\omega) \leftrightarrow \omega$. While other relationships may be necessary, this approximation is adequate for many of the cases treated in this review and, whenever necessary, other approaches will be indicated. The following notations were also used:

- $l(\omega_j)$, Eq. (7), was rewritten as

$$l(\omega_j) = i\sqrt{\frac{\hbar\omega_j}{2\varepsilon_0 n^2}} = i\sqrt{\frac{\hbar\omega_{0j}}{2\varepsilon_0 n^2}} \sqrt{\frac{\omega_j}{\omega_{0j}}} \equiv l(\omega_{0j}) \sqrt{\frac{\omega_j}{\omega_{0j}}}, \quad (38)$$

where ω_{0j} are the central frequency associated with the signal and idler luminescences and pump beam. These central frequencies obey the energy conservation $\omega_{01} + \omega_{02} = \omega_{03}$. For example, for a single-frequency laser ω_{03} , the signal and idler frequencies are related by $(\omega_{01} + \omega) + (\omega_{02} - \omega) = \omega_{03}$, that is to say, with imply balanced deviations with respect to the central frequencies.

- The spectral density function $\phi(\omega_1, \omega_2; \omega_3) \simeq \phi(\omega_{01} + \omega, \omega_{02} - \omega; \omega_{03})$ specifies the distribution of frequencies emitted from the crystal. It can be normalized^[1] with the condition $2\pi\delta\omega \sum_{\omega} |\phi(\omega_{01} + \omega, \omega_{02} - \omega; \omega_{03})|^2 = 1$. The explicit form of 4 is:

$$\phi(\omega_1, \omega_2; \omega_3) = N \prod_{j=1}^3 \sqrt{\frac{\omega_j}{\omega_{0j}}} \prod_{m=1}^3 \left[\frac{\sin\left(\frac{\Delta k_m l_m}{2}\right)}{\left(\frac{\Delta k_m l_m}{2}\right)} \right], \quad (39)$$

where N is the normalization factor.

- η includes several parameters connected with the efficiency of the down-conversion process:

$$\eta \equiv \frac{l^*(\omega_{01})l^*(\omega_{02})l(\omega_{03})}{2\pi i \hbar N (cA)^{\frac{3}{2}}} \tilde{\chi}_{ijk}^{(2)}(\mathbf{e}_{\mathbf{k}_3, s_3})_i (\mathbf{e}_{\mathbf{k}_1, s_1})_j^* (\mathbf{e}_{\mathbf{k}_2, s_2})_k^*. \quad (40)$$

In particular, η contains the field amplitudes l , that is to say, the luminescence depends *parametrically* on the field amplitudes and on the electrical susceptibility $\chi^{(2)}$. Extensive research has been dedicated to find crystals with improved coefficients $\chi^{(2)}$

This paper explores a few possibilities contained in this wavefunction. Longitudinal coherence properties have been studied in several papers but, only recently, transverse coherence properties have started to be taken into consideration.

Energy and momentum entanglements are explicitly contained in this wave function, bringing non-localization properties naturally into scene. Polarization entanglements have also been constructed in several experiments, and it has been proposed that direct polarization entanglement can be found along special

propagation directions of the twin-beams^[20], opening other paths to be explored.

1.9 Photon counting rates

The detection probability of a photo-electron in a detector of area A , placed at \mathbf{r} , between t and $t + dt$, is [16,21]

$$R(\mathbf{r}, t) dt \sim a' c A dt \langle E^{(-)}(\mathbf{r}, t) E^{(+)}(\mathbf{r}, t) \rangle, \quad (41)$$

where a' is the detector efficiency and the symbol average include both classical and quantum aver-

ages. The electrical field can be written such that $\langle E^{(-)}(\mathbf{r},t) E^{(+)}(\mathbf{r},t) \rangle$ gives the counting rate per second, that is to say, *number* per second and not energy per second. This is achieved rewriting the electrical field as

$$E^{(+)}(\mathbf{r},t) = \sqrt{\frac{\delta\omega}{2\pi}} \sum_{\omega} \hat{a}(\omega) e^{-i\omega(t-\tau)}, \quad (42)$$

where τ is the transit time from the source to the detector.

The photon counting rate will be

$$R(\mathbf{r},t) = \alpha \langle E^{(-)}(\mathbf{r},t) E^{(+)}(\mathbf{r},t) \rangle, \quad (43)$$

where $a = \alpha' \frac{A}{A_c}$ is the effective detector efficiency and A_c is the coherence area of the light field.

The quantum average performed with the wavefunction $|t\rangle$ followed by the classical average on the laser field lead to¹³

$$R(\mathbf{r},t) = a \langle t | E^{(-)}(\mathbf{r},t) E^{(+)}(\mathbf{r},t) | t \rangle = a |\eta|^2 \langle I_p \rangle, \quad (44)$$

where $\langle I_p \rangle$ is the intensity, in average number of photons per second of the pumping laser, multiplied by the crystal conversion efficiency $|\eta|^2$, giving the down-converted number of photons per second.

With Eq. (44) it is easy to obtain a condition to have a weak pumping laser:

$$\alpha |\eta|^2 \langle I_p \rangle t_{int} \ll 1. \quad (45)$$

Whenever this condition is satisfied the expansion in Eq.(37) can be safely truncated in the first order in the number of photons.

1.10 Photon coincidence rate

The conditional detection probability to have a signal photon at \mathbf{r} , at the instant t and an idler photon at \mathbf{r}_i , at $t + \tau$ is also directly calculated, leading to

$$\begin{aligned} R_{s,i}(\mathbf{r}_s, t; \mathbf{r}_i, t + \tau) &= \\ &= \alpha_s \alpha_i \langle t | E_s^{(-)}(\mathbf{r}_s, t) E_i^{(-)}(\mathbf{r}_i, t + \tau) E_i^{(+)}(\mathbf{r}_i, t + \tau) E_s^{(+)}(\mathbf{r}_s, t) | t \rangle = \alpha_s \alpha_i |\eta|^2 \langle I_p \rangle. \end{aligned} \quad (46)$$

However, the coincidence electronics associated with fast detectors has a finite resolution time T_R above which individual pulses can be identified¹⁴ or it will be able to distinguish non-coincident pulses. To obtain the coincidence rate, an integral over T_R have to be performed on $R_{s,i}$ to achieve the coincidence rate $C_{s,i}(t)$:

$$C_{s,i}(t) = \int_{-\frac{T_R}{2}}^{\frac{T_R}{2}} R_{s,i}(\mathbf{r}_s, t; \mathbf{r}_i, t + \tau) d\tau. \quad (47)$$

In a stationary regime this leads to

$$C_{s,i} \simeq \alpha_s \alpha_i |\eta|^2 \langle I_p \rangle. \quad (48)$$

This last expression reveals that the coincidence rate is proportional to the *single* intensity count, an expected result as a coincident pair will give a single coincidence count.

In case of uncorrelated photons, Eq. (46) will give the product of the correlation of the signal and idler

¹³In this calculation the substitution $\delta\omega \sum_{\omega} \rightarrow \int d\Omega$ was made and the following Dirichlet integral was used

$$\frac{1}{2\pi} \int_{-\infty}^{\infty} d\Omega e^{i\Omega(\tau - \frac{t_{int}}{2})} \frac{\sin(\frac{\Omega}{2} t_{int})}{(\frac{\Omega}{2})} = 1, \text{ for } \tau > 0.$$

The average laser intensity, in (c/s), $\langle I_p \rangle$, is given by $\frac{\delta\omega}{2\pi} \sum_{\omega} |\nu(\omega)|^2$. This quantity is identified with the number of photons around ω_p within a coherence time given by $\delta t = \frac{2\pi}{\delta\omega}$.

¹⁴The detector itself has a finite resolution time due to the flight time of photo-electrons. Two photons reaching the detector within this interval will be seen as the same event. High counts can present severe distortions due to this "pile-up" effect.

¹⁵A signature of accidental count rate in any theoretical expression is the simple proportionality dependence on T_R .

fields, leading to the accidental count rate C_A ¹⁵

$$C_A = \alpha_s \langle t | E_s^{(-)}(\mathbf{r}_s, t) E_s^{(+)}(\mathbf{r}_s, t) | t \rangle \times \alpha_i \int_{-\frac{T_R}{2}}^{\frac{T_R}{2}} \langle t | E_i^{(-)}(\mathbf{r}_i, t + \tau) E_i^{(+)}(\mathbf{r}_i, t + \tau) | t \rangle d\tau = (\alpha_s |\eta|^2 \langle I_p \rangle) \times (\alpha_i |\eta|^2 \langle I_p \rangle) T_R, \quad (49)$$

However, correlated photons as well as uncorrelated photons can be detected within a measurement time interval. A useful quantity, where accidental coincidences are subtracted, is called *relative coincidence excess* λ_E , being defined by

$$\lambda_E = \frac{C_{s,i} - C_A}{C_A} \quad (50)$$

II. Reflections of a single photon in a cavity

Consider the basic geometry illustrated in Fig. 1. For a low intensity pump the condition $(n) \ll 1$, within a coherence time, is easily achieved. The coherence time that defines the time overlap between signal and idler wavepackets, in a coincidence measurement, is given by the broader frequency bandwidth filter used before the detector. Usual interference filters have bandwidths of order $\sim 100 \text{ \AA}$ and this gives packets of order $\sim 5 \mu\text{m}$. However, the overall dead-time introduced by the detection system is a few nanoseconds and this establishes the minimum pulse definition in time.

Suppose that a Fabry-Pérot (FP) is introduced and aligned in one of the downconverted beams, say the idler beam, (See Fig. 2). In case a photon in the signal beam is used as a *start* to "time" the arrival of the conjugated idler photon, one could ask how long it would take to get the idler photon after passing through the FP cavity. In other words, for a signal photon arriving at instant t , what is the probability to get the idler photon at $t + \tau$? Calculation of Eq. (46) in section I, $R_{s,i}(\mathbf{r}_s, t; \mathbf{r}_i, t + \mathbf{r}) \equiv \mathbf{a}, \alpha_i G^{(2,2)}(\tau)$ supplies the answer. The calculation of the correlation function $G^{(2,2)}(\tau) = \langle t | E_s^{(-)}(\mathbf{r}_s, t) E_i^{(-)}(\mathbf{r}_i, t + \mathbf{r}) E_i^{(+)}(\mathbf{r}_i, t + \mathbf{r}) E_s^{(+)}(\mathbf{r}_s, t) | t \rangle$ is developed in Ref. [22], and a simple answer is obtained as

$$G^{(2,2)}(\tau) = \sum_{m=0}^{\infty} r^{4m} |\chi_0(\tau - \tau_{2m+1})|^2, \quad (51)$$

where r is the FP cavity's mirror reflection coefficient and $\chi_0(t)$ is the Fourier transform of the spectral function ϕ .

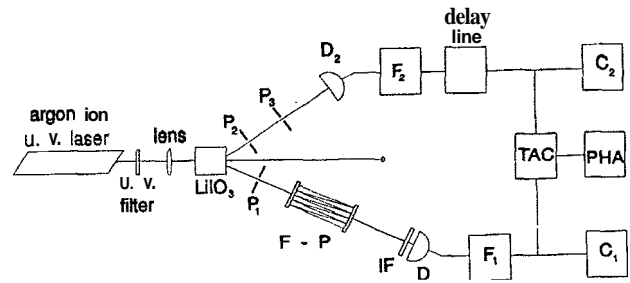


Figure 2. Experimental setup for detection of a conjugated beam after passing through a Fabry-Pérot cavity. Detector D_2 sends a *start* pulse that will be followed by a stop pulse from detector D_1 after some delay time.

The experimental result is shown by the dots in Fig. 3 and the theoretical prediction is given by the solid vertical lines. The large width of the experimental peaks actually represents the instrumental dead-time. One can see that the experimental results also shows faster decaying peaks than the theory; the explanation for this fact is that the theory is not considering the existing divergence of the idler beam but only the decaying probability to have a photon transmitted along the time.

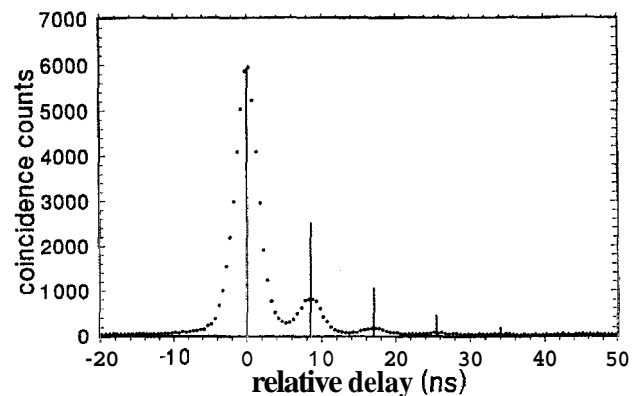


Figure 3. Coincidence counts versus the delay time. The origin is set at the first photon pass through the cavity. Subsequent pulses are second, third photon pass, and so on. Time between passes is 8.5 ns, a round-trip pass within a 1.275 m long cavity.

The interpretation of the experimental result of a series of peaks is that the first pulse is connected with a successful photon transmission in its first pass by the FP cavity, the second one shows a successful transmission after reflections by the output mirror and the input mirror in time $2 \times \tau_1$, where τ_1 is the cavity transit time, and so on.

This experiment shows the effect of the cavity inserted along a broad frequency wavepacket: The cavity

defines a much narrower frequency bandwidth and, consequently, increases the coherence time at the output. This longer coherence time is reflected in the envelope of the peaks - one doesn't know in each peak a photon will be detected within that envelope.

III. Induced coherence without stimulated emission

The understanding that the concepts of degree of coherence in optics and degree of indistinguishability of light paths are, in reality, identical concepts, may simplify our comprehension of many phenomena. This relationship^[23] is supported by several recent experiments^[1] using parametrically down-converted light. The phenomenon of *induced* coherence *without* stimulated emission, with no classical counterpart, has been one of the experimental grounds on which that relationship has been tested using down-converted light.

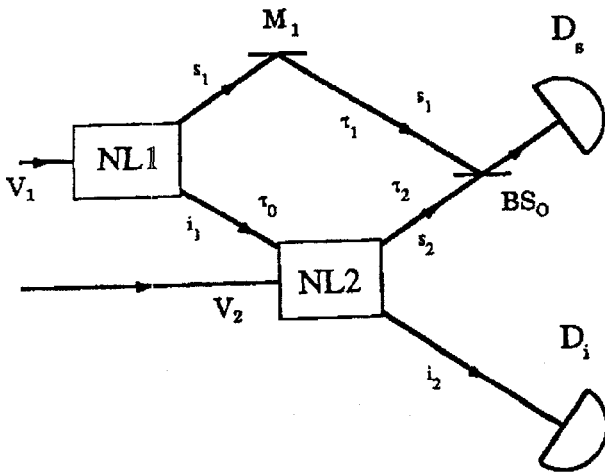


Figure 4. Basic outline of the experiments. NL1 and NL2 are the two χ^2 nonlinear crystals pumped by the two classical field amplitudes V_1 and V_2 . Signal beams S_1 and S_2 are superposed on the beam splitter BS_0 and collected by detector D_s . Idler beams are collected by detector D_i .

This phenomenon refers to experiments showing interference between the signal beams spontaneously emitted by two crystals when their idler conjugate beams are collinearly superposed and the path followed by the detected signal photon cannot be identified. The basic geometry utilized in those experiments is shown in Fig. 4. Several alignment pinholes used after the

crystals are not shown. The idea is that the alternative routes of the signal photons cannot be identified by measurements and, consequently, they are *indistinguishable* in principle - that is why the interference appears. (The reader could try to devise a measurement to identify the photon route without destroying the visibility). The degree of visibility achieved in these experiments plays a crucial role in the understanding of that phenomenon; a special characteristic is that the visibility is not dependent on the intensity of the idler beam inducing coherence.

The interference is measured varying the position of the BS_0 beam-splitter using a piezo-electric translation stage. A typical interference pattern is shown in Fig. 5. Displacement calibration can be done with a laser of known wavelength. A single mode laser beam split by a 50/50 beam splitter was used to pump the two crystals¹⁶. The theoretical visibility of the intensity correlation can be calculated in a straightforward manner^[1] and it gives

$$v = \frac{2|\eta_1\eta_2| \sqrt{\langle I_1 I_2 \rangle}}{|\eta_1|^2 \langle I_1 \rangle + |\eta_2|^2 \langle I_2 \rangle} |\gamma_{12}| |\gamma_s(\tau_0 + \tau_2 - \tau_1)|, \quad (52)$$

where $\langle I_1 \rangle$ and $\langle I_2 \rangle$ are the average pump laser intensities, and $|\eta_1|^2$ and $|\eta_2|^2$ are the down-conversion efficiencies for each crystal. γ_{12} is the second order cross-correlation function of the pump beams and $\gamma_s(\tau_0 + \tau_2 - \tau_1)$ is the normalized auto-correlation function of the down-converted signal light. τ_1 , τ_2 , and τ_0 are, respectively, the optical propagation times from crystal 1 to beam-splitter BS_0 along the signal 1 path, from crystal 2 to beam-splitter BS_0 along the signal 2 path, and from crystal 1 to crystal 2 along the idler 1 path.

When the interferometer path lengths are balanced with respect to the *longitudinal* coherence of the down-converted beams, $\tau_0 = \tau_1 - \tau_2$, then $|\gamma_s(\tau_0 + \tau_2 - \tau_1)| = 1$. The coherence length of the pump laser beam is such that $|\gamma_{12}| \approx 1$. A large visibility should then be expected in the experiments when $|\eta_1|^2 \langle I_1 \rangle = |\eta_2|^2 \langle I_2 \rangle$.

The two crystals can be seen as analogous to the two slits in a Young experiment. Any means that might change the indistinguishability of the idler photons coming from crystal 1 or crystal 2 will affect the resulting visibility obtained from interference fringes

¹⁶A single mode pump laser is not necessary for these experiments.

formed with the signal photons. For example, a drastic blocking of the idler beam from crystal 1 before it reaches crystal 2 destroys immediately the interference pattern between the signal beams; for example, a coincidence measurement between D_s and D_i would guarantee that crystal 2 is the source of the photon pair - the photon path becomes *distinguishable*!

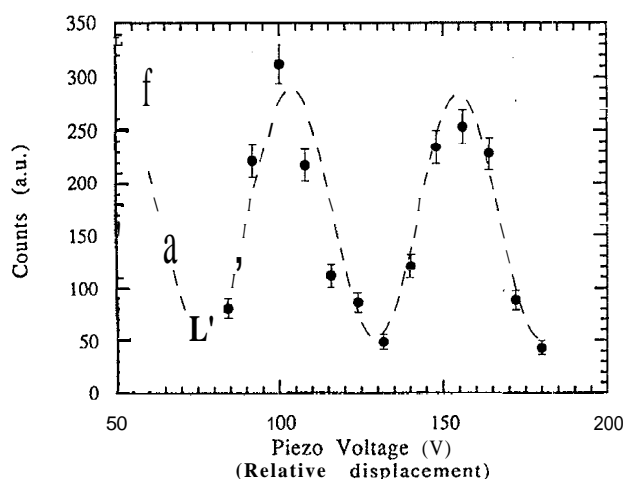


Figure 5. A typical interference pattern obtained in coincidence measurements with collinearly aligned idler beams. Measured visibility \mathcal{V} is 69%.

It is important to note that the visibility control can be done *without* intensity changes in the signal beams, or in its frequency spectral density. The control of visibility between two beams is of interest to several areas as optical communication, optical computing and integrated optics. The control mechanism in this case is purely quantum mechanical, with no classical analog. Besides a practical interest associated with this effect, one should not underestimate the basic study of the phenomenon itself.

The visibility could also be drastically reduced, of course, by an incorrect alignment of the idler beams through the second crystal or of the signal beams at the interferometer beam splitter^[24], or even due to thermal or mechanical instabilities, as in any interferometer. Anyway, in all experiments the overall conditions are controlled so that one is close to an ideal case. However, even with a strict control of all these conditions, and with no time delays or losses in the idler 1 beam path connection, the measured visibilities are found to be well below the ideal value of 1 in several experiments that were performed under non-identical geometries, pinhole arrangements etc. The values of

the fourth order or coincidence visibility \mathcal{V} were never appreciably above 70%. How to explain this mismatch between the theoretical prediction and the experimental values? As a new phenomenon under study, some effort has to be made towards this understanding.

It was found^[25] that those reduced values of the visibility can be explained, in a heuristic way, applying the ideas of *induced transverse* degree of coherence and the degree of transverse *spatial overlap* between the two aligned beams. These two ideas will be shown separately, for clarity, and combined afterwards.

III.1 The "induced transverse" degree of coherence

The spontaneously emitted down-converted light has a very short coherence time t_c ($< 10^{-13}$ sec), corresponding to a short coherence length l_c ($< 5 \mu\text{m}$). The emitted light from the crystal will be idealized as a superposition of light emitted from uncorrelated thin crystal slabs of thickness l . The separation R between the crystals 1 and 2 along the aligned connection path is such that $l_c \ll R$. Fig. 6 shows two slabs separated by a distance R and emitting collinearly aligned light.

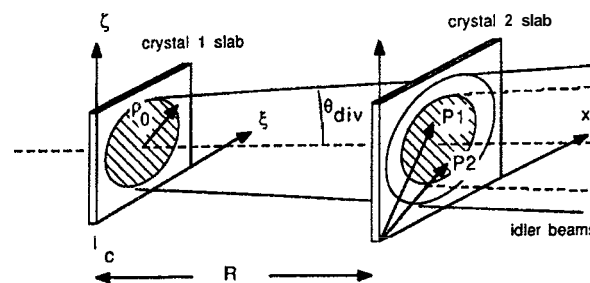


Figure 6. Emitting slabs in crystals 1 and 2. Collinearly aligned idler beams are shown. R is the separation between the two crystals and θ_{div} is the $1/e^2$ divergence of the down-converted light.

While signal photons emitted from crystal 1 and crystal 2 have intensities $\langle I_{s1} \rangle = |\eta_1|^2 \langle I_1 \rangle$ and $\langle I_{s2} \rangle = |\eta_2|^2 \langle I_2 \rangle$, the measured coincidence visibility will be determined by the fraction of emitted photons from crystal 2 *correlated* with respect to the idler photons from crystal 1. The correlated fraction of the signal beam from crystal 2, with a *definite* phase relationship with the signal beam from crystal 1, will produce interference.

Although not being isotropic emitters, each slab will be further idealized as a finite thermal-like source composed of spatial incoherently emitting points. The idler light emitted by each slab of crystal 1 will have a second order correlation function $\Gamma(\mathbf{P}_1, \mathbf{P}_2, t_1, t_2) = \langle E_1^-(\mathbf{P}_1, t_1) E_1^+(\mathbf{P}_2, t_2) \rangle$, between any two points \mathbf{P}_1 and \mathbf{P}_2 on a similar slab of crystal 2. See Fig. 7. The propagation of the correlation function $\Gamma(\mathbf{r}_1, \mathbf{r}_2, t_1, t_2)$,

in a stationary state, is given by the wave equation^[26]

$$\nabla^2 \Gamma - \frac{1}{c^2} \frac{\partial^2 \Gamma}{\partial \tau^2} = 0, \quad (53)$$

where $\alpha = 1, 2$ and $\tau = t_2 - t_1$. The solution of this equation is known for the case of a quasi-monochromatic, incoherent source and is expressed by the classical Van Cittert-Zernike theorem^[26],

$$\Gamma(\mathbf{P}_1, \mathbf{P}_2, \tau) \cong \left(\frac{k_i}{2\pi}\right)^2 \frac{e^{i(\psi + \omega_i \tau)}}{R^2} \int_{\sigma_1} |\eta_1|^2 I_1(\xi, \zeta) e^{-ik_i(p\xi + q\zeta)} d\xi d\zeta, \quad (54)$$

where $p = \frac{x_2 - x_1}{R}$ and $q = \frac{y_2 - y_1}{R}$ are associated with points $\mathbf{P}_1, \mathbf{P}_2$ on a slab of crystal 2. k_i and ω_i specify the wavevector amplitude and angular frequency of the idler light. $|\eta_1|^2$ is the down-conversion efficiency and $I_1(\xi, \zeta)$ is the pump intensity in the slab of crystal 1, that will be idealized as spatially uncorrelated. In this case, the coherence area at crystal 2 of light emitted by a circular slab in crystal 1 can be estimated from the first zero of the normalized Γ correlation function^[26]

$$\gamma(\mathbf{P}_1, \mathbf{P}_2, \tau) = e^{i(\psi + \omega_i \tau)} 2 \frac{J_1\left(\frac{k_i \varrho_0 |\Delta \mathbf{P}|}{R}\right)}{\left(\frac{k_i \varrho_0 |\Delta \mathbf{P}|}{R}\right)}, \quad (55)$$

giving a coherence area

$$A_{\text{coh}1 \rightarrow 2} \cong 0.29 \left(\frac{R \lambda_i}{\varrho_0}\right)^2, \quad (56)$$

where ϱ_0 is the $1/e^2$ radius of the pump beam and is assumed to be the same at each crystal. The fraction f of this area to the slab source area at crystal 2, given by $A_2 = \pi \varrho_0^2$, is

$$f = \frac{A_{\text{coh}1 \rightarrow 2}}{A_2} \cong \frac{0.29 (R \lambda_i)^2}{\pi \varrho_0^4}. \quad (57)$$

For typical values of the parameters $R \cong 25$ cm, $\varrho_0 \cong .035$ cm and $\lambda_i \cong 7900 \text{ \AA}$, this gives $f \cong 0.24$. Consequently, within the total intensity $|\eta_2|^2 I_2$ produced by crystal 2, only the fraction $f |\eta_2|^2 I_2$ would have originated within one coherence area of the light emitted from crystal 1. Eq. (52) can then be modified to include this fraction f ,

$$\vartheta = 2 \frac{\sqrt{|\eta_1|^2 \langle I_1 \rangle (f |\eta_2|^2 \langle I_2 \rangle)}}{|\eta_1|^2 \langle I_1 \rangle + (f |\eta_2|^2 \langle I_2 \rangle)} |\gamma_{12}| |\gamma_s(\tau_0 + \tau_2 - \tau_1)|. \quad (58)$$

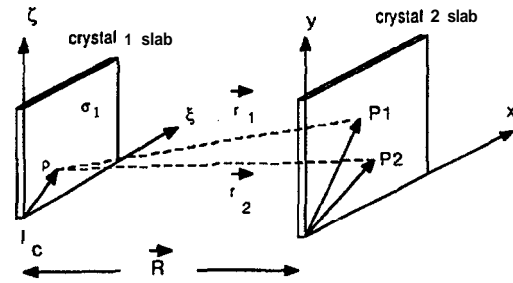


Figure 7. Geometry used to calculate the first order correlation function for the signal light from crystal 1 between points \mathbf{P}_1 and \mathbf{P}_2 over a slab of crystal 2.

Even under ideal alignment conditions with $|\gamma_{12}| = |\gamma_s| = 1$ and $|\eta_1|^2 \langle I_1 \rangle = |\eta_2|^2 \langle I_2 \rangle$, this gives

$$\vartheta \cong \frac{2\sqrt{f}}{1+f} \cong 0.79, \quad (59)$$

that is to say, $\vartheta \cong 79\%$ is an upper bound on the experimental visibility if only the transverse coherence plays a role.

III.2 Degree of overlap between the two idler beams. Combined corrections.

Under ideal conditions of collinearly aligned idler beams, while any increase in the distance R between crystal 1 and crystal 2 leads to a desirable increase in the coherence area fraction of idler beam 1 over crystal 2, as shown by Eq. (56), the overlap between the source area in crystal 2 and the total idler beam emitted by

crystal 1 decreases. (See Fig. 6). This decrease in the overlap leads to an increased distinguishability of the two beams, as one could see by placing an imaginary detector with a very small aperture in the idler path immediately after crystal 2. It would then be possible, in principle, to identify a fraction of the light coming with certainty from crystal 1.

The ratio r of the source area, $(\pi \varrho_0^2)$, on crystal 2 to the idler emission area from crystal 1 projected on crystal 2, $A_{1(2)} = \pi(\varrho_0 + R\theta_{div})^2$, gives the indistinguishable fraction of light,

$$r = \frac{\varrho_0^2}{(\varrho_0 + R\theta_{div})^2}, \quad (60)$$

where θ_{div} is the divergence angle of idler 1.

This ratio r will further modify the expression for the visibility given by Eq. (58) because signal 1 photons corresponding to the distinguishable portion of the idler 1 beam will not take part to induce coherence. Combining these corrections, the upper bound for the visibility will then be

$$\vartheta = \frac{2\sqrt{fr}}{1 + fr} \quad (61)$$

The experimental parameters for the data shown in Fig. 5 give $f \cong 0.24$ and $r \cong 0.6$ ($\theta_{div} \cong .4$ mrad). With these values, Eq. (61) gives $\vartheta \cong 0.67$; this agrees within the uncertainties with the experimental value of visibility shown in Fig. 5, where $\vartheta \cong 0.69 \pm 0.09$.

While this expression explains what is causing the low values of the visibility one cannot improve ϑ arbitrarily. For example, to increase the separation between the two crystals R such that the coherence area is much larger than the illuminated region in crystal 2 will not improve the visibility too much and the fraction f will be further decreased. It should be noted that single channel interferences shows an even lower degree of visibility. (See Fig. 8).

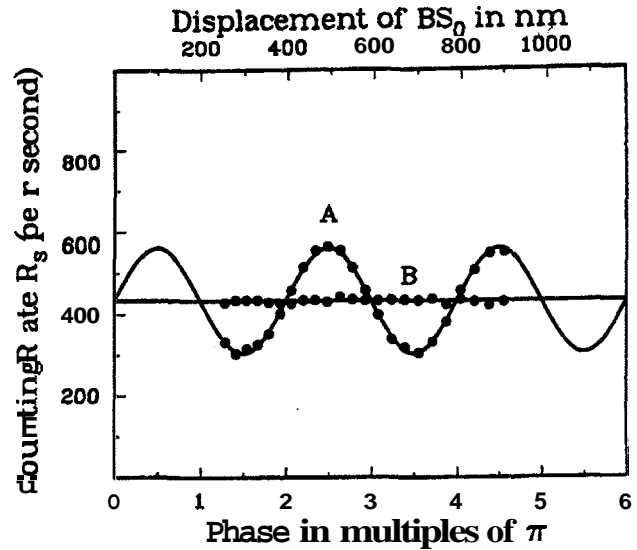


Figure 8. Single channel interference fringes in a typical PZT sweep (From Wang et al, in Ref.(1)).

Imperfections such inadequate anti-reflective coating on crystal 1 and crystal 2 would further reduce the measured visibility. Extreme care has to be taken in an experiment to bring the conditions close to the ones supposed in the theory.

11.3 Other questions

The modifications introduced in the expression for the visibility by these heuristic arguments lead to a reasonable agreement with the experiment. Besides this explanation, some questions could be forwarded, like: How one could improve the visibility degree or, in other words, how to increase the degree of indistinguishability between the idler beams? Another question concerns the basic understanding of the physical mechanism establishing the phase correlation between the two signals at the level of the crystal 2 emission. The process leading to an *induced phase* relationship between the signal beams from crystal 1 and 2 has a subtle character, as the emission from crystal 2 is *spontaneous* and yet, somehow, it is connected with the idler emission from the crystal 1. An important point to be observed is that the degree of visibility do not depend on the number of photons in the idler connection, even a very low photon number rate may lead to the same degree of visibility of more intense beams.

IV. Visibility control

Since the crystal 2 decays spontaneously one should understand what is the physical mechanism that locks the phase of the signal beams from crystal 1 and crystal 2. It was shown that a blocking of the idler 1 destroys the interference between the signal beams although the intensity of these beams are not affected by modifications introduced in the idler path. Coincidence measurements taken between detector D_s and a detector D_i placed after crystal 2 along the idler beams would show coincidence only between photon pairs emitted from crystal 2; in this way the signal photon path can be identified. The degree of distinguishability is therefore maximum and the coherence between signal 1 and signal 2 disappears.

A partial blocking of the idler connection path, such as done by a neutral density filter, also leads to a decrease in the visibility^[1]. This decrease is related not to the lower intensity of the idler beam after the neutral filter but to the increased degree of distinguishability introduced by that filter: A similar coincidence measurement taken between detector D_s and detector D_i would show a decreasing coincidence rates as the neutral filtering is increased; this shows an increased distinguishability of the signal beams and, eventually, becomes a maximum when the filter blocks 100 % of the idler beam from crystal 1.

The study of the phase mechanism locking the signal beams to the same phase led to an extended search of ways of controlling the visibility through changes in the idler connection path.

A. Phase delays

One of the studies of visibility control utilized a series of glass plates, of calibrated width and anti-reflecting coated to minimize any light loss, introduced in the idler connection path^[27]. (See Fig 9). A glass plate introduces a time delay T for the light beam, proportional to its thickness. As was already discussed, the down-converted beams have wavepackets with coherence time τ_c ; depending of the interference filters utilized. Suppose that a glass plate delays the signal beam from crystal 1 by T . If the detector D_i is placed at the same distance from crystal 2 than detector D_s , a coincidence seen with no time delay between D_s and D_i

will assure that the photon pair originates from crystal 2. It should be remembered that this is a balanced interferometer with length $NL1 - A4I - BS_0$ equal to $NL1 - NL2 - BS_0$.

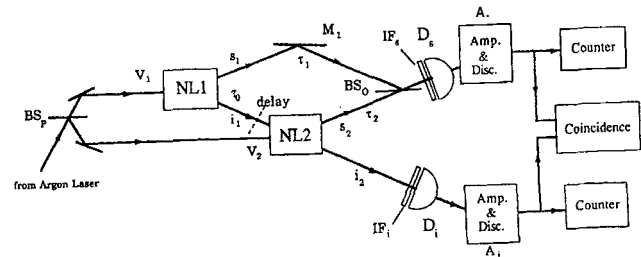


Figure 9. Experimental setup with a phase delay introduced in the idler connection path.

Setting detector D_s as the start detector and D_i as the stop, if the coincidence is seen after detector D_i is delayed by $T \gg \tau_c$ with respect to D_s , this will assure that the photon pair comes from crystal 1. This corresponds to a distinguishability of the signal photon paths and, consequently, to the vanishing of the coherence between the signal beams from crystal 1 and 2. Of course, an intermediate situation is seen for $T \sim \tau_c$. In this case the visibility obtained from the interference patterns should go from a maximum value, with no delay, to a vanishing value with a maximum delay introduced by the thickest glass plate utilized. Fig. 10 shows the visibility values obtained in function of the delays introduced by the low-loss calibrated thickness glass plates.

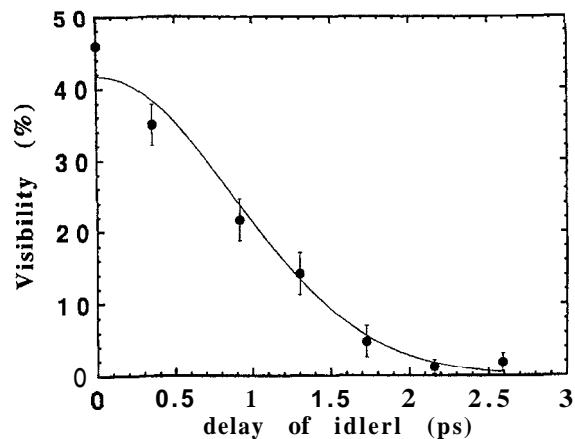


Figure 10. Visibility values obtained from the interference patterns on BS_0 as a function of the differential time delay T in ps. Solid curve is a fit to $V = \text{constant} \times e^{-t^2/2\sigma_L^2}$.

Another way to understand this result is by analysis of the signal beams. Assume that the pump beams have

the same phase as they reach crystals 1 and 2 and that the down-conversion process is very fast - the crystal excitation happens in a virtual process. As an experimental result we know that the signal phases are locked due to the idler connection and they are unlocked if the idler connection is blocked. With a lossless glass plate in the idler 1 beam producing a delay $T \leq \tau_c$, the down-converted signal wavepackets will be overlapping and interfering on BS_0 . As T becomes appreciably larger than τ_c the overlap vanishes and so does the interference.

Solid line in Fig. 10 was obtained along these ideas. The spectral weight function $\phi(\omega_s, \omega_i; \omega_p)$ presents a quite broad spectra but, in practice, the measured ϕ is restricted by the interference filters used. If one write this measured ϕ as $\phi_m(\omega, \omega_p - \omega; \omega_p)$ or simply $\phi_m(\omega, \omega_p - \omega)$, the autocorrelation function of the down-converted light will be

$$g(\tau) = \frac{1}{2\pi} \int_0^{\omega_p} |\phi_m(\omega, \omega_p - \omega)|^2 e^{-i\omega\tau} d\omega. \quad (62)$$

The Fourier transform of the spectral function, $z(\tau)$, gives the wavepackets associated with the down-converted light:

$$z(\tau) \equiv \frac{1}{2\pi} \int_0^{\infty} \phi_m(\omega, \omega_p - \omega) e^{-i\omega\tau} d\omega. \quad (63)$$

It is quite natural to define the degree of indistinguishability D between the two signal photon paths, $s1$ and $s2$, as the normalized overlap of the signal (or idler) wavepackets as

$$D \equiv \frac{|\int_{-\infty}^{\infty} z_{s1}^*(\tau) z_{s2}(\tau + T) d\tau|}{\int_{-\infty}^{\infty} |z(\tau)|^2 d\tau}, \quad (64)$$

where $z_{s1} = z_{s2} = z$ for $T = 0$.

Substituting the above definition of $z(\tau)$ in this equation leads directly to

$$D = \frac{|g(T)|}{g(0)} = |g(T)| \quad (65)$$

This result is an explicit statement that the degree of indistinguishability D of the photon wavepackets (or photon paths) is the degree of coherence $|g(T)|$ of the down-converted field.

With an interference filter of Gaussian frequency passband defining the spectral shape of ϕ_m , one gets

$D \propto \vartheta \propto \exp(-l^2/2\sigma_L^2)$, where l is the optical path difference and σ_L is the wavepacket coherence length. The solid line in Fig. 10 is a fit to this expression.

B. Berry's phase modulation on the visibility

Trying to increase the knowledge about control of the interference between signal photons through the idler connection path, an experiment^[28] was performed with the introduction of a geometrical phase shift in that path. The geometrical phase shift, also known as Berry's phase^[29] in a general sense or, by Pancharatnam's phase in the optical domain^[30], was chosen due to the absence of dynamical effects in it.

This phase shift is done in a closed cycle of some chosen parameter of the Hamiltonian for the process under study. Suppose this parameter is being changed in a cyclic variation from $t = 0$ to $t = \tau$. The Hamiltonian $\hat{\mathcal{H}}(t)$ describing this cyclic process is such that $\hat{\mathcal{H}}(0) = \hat{\mathcal{H}}(\tau)$. The wavefunction is given by

$$|\psi(\tau)\rangle = \exp\left(i\frac{\hat{\mathcal{H}}(\tau)}{\hbar}\right) |\psi(0)\rangle \equiv e^{i\phi_0} |\psi(0)\rangle. \quad (66)$$

The wavefunction at $t = \tau$ and $t = 0$ differs by a phase ϕ_0 . This phase contains a dynamic contribution and a geometrical one. The geometrical part is Berry's phase. In the experiment performed^[28] the geometrical contribution was separated using a polarization cycle introduced in the idler connection path, without any change in polarization of the signal beams.

Fig. 11 shows the system introduced in the connection path to produce a complete cycle in the idler polarization. Idler 1 beam, polarized horizontally in the plane of the paper pass through a beam-splitter BS_i (reflectivity and transmissivity R and T) and two quarter-wave plates. The first one, QW_1 , is set at 45° with respect to the initial idler polarization at point (1), producing (\$) circularly polarized light at its output (point 2). The optical axis of the second plate, QW_2 , can be oriented at an arbitrary angle θ with respect to the initial idler polarization; the output light is linear but oriented 2θ with respect to the original idler polarization (point 3). After reflection in mirror M_i the beam passes again through QW_2 producing (-) circularly polarized light (point 4). After passing again,

in the reversed sense, through QW_1 , the beam is again polarized along the original polarization (point 1).

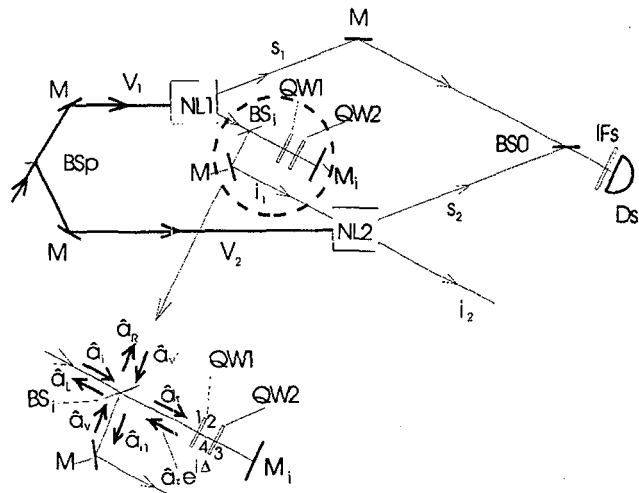


Figure 11. Optical system introduced in the connection path to produce a complete polarization cycle. Idler 1 beam, polarized horizontally in the plane of the paper is transmitted through a beam-splitter BS_i (reflectivity and transmissivity R and T), quarter-wave plates QW_1 and QW_2 and is, finally, again reflected by BS_i . The output polarization is identical to the input one.

No modification is introduced in the system besides this complete geometric polarization cycle. Each step of this cycle has a simple geometric visualization as geodesic lines on a Poincaré's sphere^[31]. Berry's phase β can be shown^[29] to be equal to 2θ . This shows a signature of a Berry's phase: varying QW_2 by θ , any measured effect should result proportional to 2θ .

Fig. 12 shows the measured interference pattern obtained by translating BS_0 with a PZT translation stage

when the optic axis of the waveplate QW_2 is set at 0 with respect to the initial idler polarization. Observe that when θ changes by π a complete interference cycle of 2π is obtained. The visibility obtained from the signal counting rate R_s data is

$$v = \frac{R_{s,max} - R_{s,min}}{R_{s,max} + R_{s,min}} \cong (12 \pm 1)\% . \quad (67)$$

This value is even lower than the ones obtained in the experiments of "induced coherence without stimulated emission", despite a strict control of vibrations, temperature fluctuations and good optical alignment. This decrease in visibility can be explained with a simple application of the basic single-mode theory from Section I:

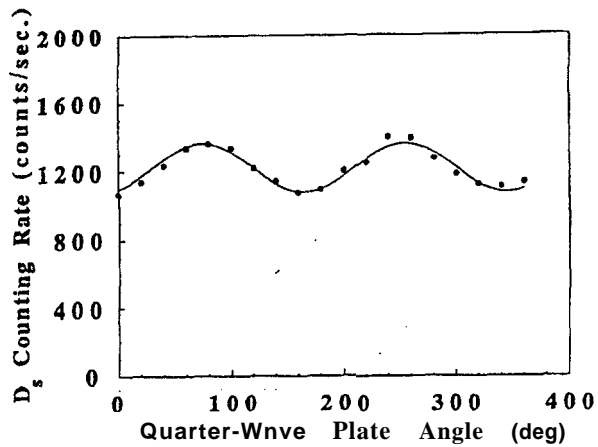


Figure 12. Interference seen as the optic axis of the waveplate QW_2 is changed by θ with respect to the initial idler polarization. A complete interference cycle of 2π is obtained when θ changes by π .

Our aim is to calculate the superposed electric field \hat{E}_s at the beam-splitter BS_0 and the expected value R_s , given by Eq. (43):

$$R_s = \alpha_s \langle t | \hat{E}_s^{(-)}(t) \hat{E}_s^{(+)}(t) | t \rangle , \quad (68)$$

from which the visibility v , Eq. (67), is obtained. The indicated average assumes that whenever classical quantities are involved an appropriated classical average is performed.

The interaction term \hat{V} in the single-mode Hamiltonian, Eq. (11), from a process with crystals 1 and 2, will be written

$$\hat{V} = \sum_{j=1}^2 \hat{V}_j , \text{ where} \quad (69)$$

$$\hat{V}_j = \hbar g_j v_j \hat{a}_{s_j}^\dagger \hat{a}_{i_j}^\dagger + H.c. , \quad (70)$$

the indexes 1 and 2 stands for crystals 1 and 2.

The wavefunction at time t , $|t\rangle$, in a weak pump beam condition, is given by

$$|t\rangle = e^{-i\int_0^t \hat{V} dt} |0\rangle \cong (1 - i\frac{\hat{V}t}{\hbar}) |0\rangle = |0\rangle - it \left[g_1 v_1(t) \hat{a}_{s1}^\dagger \hat{a}_{i1}^\dagger + v_2 \hat{a}_{s2}^\dagger \hat{a}_{i2}^\dagger \right] |0\rangle. \quad (71)$$

It should be observed that \hat{a}_{i2}^\dagger at the beam splitter BS_0 will be set equal to \hat{a}_{i1}^\dagger defined after the Berry's phase optical elements - the *indistinguishability* condition. The mismatch between coherence areas, and superposed fields as discussed in Section III will be ignored. However, a connection has to be made between the annihilation operator for the idler beam emitted by crystal 1 and \hat{a}_{i1} , due to the losses introduced at BS_i and phase changes introduced by the extra optical elements. For the moment the annihilation operator specifying the field emitted from crystal 1 will be written without the j index: \hat{a}_i .

A generic "single surface" symmetric beam-splitter can be treated as a linear two-port device¹⁷ [32] with input operators \hat{a}_1 and \hat{a}_2 and output \hat{b}_1 and \hat{b}_2 :

$$\begin{pmatrix} \hat{b}_1 \\ \hat{b}_2 \end{pmatrix} = \begin{pmatrix} t & r \\ r & t \end{pmatrix} \begin{pmatrix} \hat{a}_1 \\ \hat{a}_2 \end{pmatrix} \quad (72)$$

The inset in Fig. 11 shows beam-splitter BS_i with inputs \hat{a}_i and \hat{a}_v , where the index v stands for a vacuum input. The outputs are \hat{a}_T and \hat{a}_R . The same inset shows the situation in BS_i after reflection by the quarter-waves and mirror M . A represents the overall phase shift acquired by \hat{a}_T in the round trip propaga-

tion from and to BS_i . \hat{a}_{i1} is the idler beam sent to crystal 2, \hat{a}_L represents a "lost" beam and $\hat{a}_{v'}$ represents another vacuum input. These processes can be written as

$$\begin{pmatrix} \hat{a}_T \\ \hat{a}_R \end{pmatrix} = \begin{pmatrix} T & \mathcal{R} \\ \mathcal{R} & T \end{pmatrix} \begin{pmatrix} \hat{a}_i \\ \hat{a}_v \end{pmatrix} \quad (73)$$

and

$$\begin{pmatrix} \hat{a}_L \\ \hat{a}_{i1} \end{pmatrix} = \begin{pmatrix} T & \mathcal{R} \\ \mathcal{R} & T \end{pmatrix} \begin{pmatrix} \hat{a}_T e^{i\Delta} \\ \hat{a}_{v'} \end{pmatrix}. \quad (74)$$

$|T|^2 + |R|^2 = 1$ and $T\mathcal{R}^* + T^*\mathcal{R} = 0$ are satisfied^[32] on the beam-splitter, where the phases acquired at the reflection and transmission obeys the condition $\phi_T - \phi_R = \pm\frac{\pi}{2}$. Δ contains Berry's phase $\beta(\theta)$ and the phase related to the optical path of total length L : $A = \beta + k_i L$, where $k_i = 2\pi/\lambda_i$.

Eqs. (73) and (74) give

$$\hat{a}_{i1} = \hat{a}_{i2} = \mathcal{R}T e^{i\Delta} \hat{a}_i + \mathcal{R}^2 e^{i\Delta} \hat{a}_v + T \hat{a}_{v'}. \quad (75)$$

Substituting Eq.(75) in the wavefunction and rewriting $\hat{a}_i \rightarrow \hat{a}_{i1}$, one obtains

$$|t\rangle \cong (1 - i\frac{\hat{V}t}{\hbar}) |0\rangle = |0\rangle - it \left[g_1 v_1(t) \hat{a}_{s1}^\dagger \hat{a}_{i1}^\dagger + g_2 v_2(t - \tau_0) \hat{a}_{s2}^\dagger \left(\mathcal{R}^* T^* e^{-i\Delta} \hat{a}_{i1}^\dagger + \mathcal{R}^* e^{-i\Delta} \hat{a}_v^\dagger + T^* \hat{a}_{v'}^\dagger \right) \right] |0\rangle. \quad (76)$$

Denoting BS_0 's transmissivity and reflectivity by ρ_0 and τ_0 , where $|\rho_0|^2 + |\tau_0|^2 = 1$, the superposed electrical field after BS_0 is

$$\hat{E}_s^{(+)} = \rho_0 \hat{a}_{s1} e^{i\phi_1} + \tau_0 \hat{a}_{s2} e^{i\phi_2}. \quad (77)$$

With these results it is straightforward to obtain $R_s(t)$, as given by Eq. (68):

$$R_s = \alpha_s \langle t | \hat{E}_s^{(-)}(t) \hat{E}_s^{(+)}(t) | t \rangle = \alpha_s \left(\hat{E}_s^{(+)}(t) | t \rangle \right)^\dagger \hat{E}_s^{(+)}(t) | t \rangle = \quad (78)$$

$$= t^2 (|\rho_0|^2 |g_1|^2 \langle |v_1(t)|^2 \rangle_{class.} + |\tau_0|^2 |g_2|^2 \langle |v_2(t - \tau_0)|^2 \rangle_{class.}) + 2t^2 \text{real} \left[\rho_0 \tau_0^* g_1 g_2^* \mathcal{R} T e^{i(\phi_1 - \phi_2 + \Delta)} \langle v_1(t) v_2^*(t + \tau_0) \rangle_{class.} \right]. \quad (79)$$

¹⁷Section VII on "Beam-splitters, cavities..." presents a concise view of this approach.

Writing $tg_j \equiv f_j$, γ_{12} as the normalized correlation function of the pump lasers at the crystals 1 and 2, representing all complex quantities z as $z = |z| e^{i\phi_z}$, and grouping all the phases together, the visibility \mathcal{V} is obtained as

$$\mathcal{V} \equiv \frac{(R_s)_{\max} - (R_s)_{\min}}{(R_s)_{\max} + (R_s)_{\min}} = \frac{2 |f_1 f_2| \sqrt{\langle I_1 \rangle \langle I_2 \rangle} |\gamma_{12}|}{\frac{\rho_0}{\tau_0} |f_1|^2 \langle I_1 \rangle + \frac{\tau_0}{\rho_0} |f_2|^2 \langle I_2 \rangle} |\mathcal{R}| |\mathcal{T}| \quad (80)$$

The factor $|\mathcal{R}| |\mathcal{T}| \sim (\frac{1}{2} \times \frac{1}{2})$ shows correctly the low visibility obtained compared to cases where no beam-splitter is inserted in the idler connection. (See Eq. (52)).

Within a distinguishability view, one could say that placing an auxiliary detector at the lost beam \hat{a}_L path, coincidence counts between this detector and D_s detector would reveal non-interfering signal photons or, in other terms, a distinguishable situation that leads to a decrease in the visibility.

V. Forced indistinguishability in "induced coherence without stimulated emission".

The reduced visibility obtained in all experiments so far performed raises the question whether these values could be, somewhat, increased. This section analyzes the non-classical phenomenon of "induced coherence without stimulated emission" under the condition where two nonlinear $\chi^{(2)}$ crystals are aligned in such a way that their idler emissions are collinear and *inside* a ring-like cavity with loss. It is shown that this configuration establishes a forced indistinguishability of the idler photons and produces an interference between the free traveling conjugated signal beams when they are superposed. This interference is found to be *independent* of the cavity loss, within the limits of a single mode theory, and highly *dependent* on the position of the crystals inside the cavity. The maximum theoretically obtainable visibility is 100%, reflecting the induced coherence in the two crystals by the cavity field. Some preliminary experimental results are discussed, stressing the difficulties involved to obtain high values of the visibility \mathcal{V} .

In all the experiments already performed, some were discussed in the former sections, the variations introduced in the connection path deliberately decreased the degree of indistinguishability and, consequently, the degree of coherence.

This section discusses a different route, namely, the situation where the idler connective path is placed within a single-mode cavity. Therefore, without destroying

this single-mode cavity geometry, it is not possible to identify the crystal from which the idler is emitted. The signal emission from the two crystals should then reflect a *forced* indistinguishability of the idler photons generated by the crystals^[33].

To better explain the idea behind this *forced* indistinguishability one should observe that in Mandel's experiments^[1], the theory was applied considering the *longitudinal* coherence of the beams necessary to produce temporally overlapping wavepackets. However, their *transverse* coherence properties were not explicitly taken into account in the experiments or within the theory developed. This is a crucial point to the comparison between theory and the experimental values of the second order visibilities $\mathcal{V}^{(2)}$. By definition, photons are indistinguishable when they are within a *coherence volume* and being longitudinally coherent it is not a sufficient condition to assure their indistinguishability. In this sense, the second order visibility $\mathcal{V}^{(2)}$ should be expected, theoretically or experimentally, to be $\mathcal{V}^{(2)} < 1$; this was discussed in Sec. IV.

This point could be further clarified by the following imaginary experiment performed on the configurations described in Ref. [1]. Assume that the separation between crystal 1 and crystal 2 is L . Placing Young double slits between crystal 2 and the idler detector, at a finite distance d from crystal 2, a fringe pattern may be seen by scanning the detector normally to the idler beam. The visibility degree obtained from the interference pattern will be below 100% as the distances between each crystal and the Young slits, $L+d$ and d , are different and, consequently, their coherence transverse areas at the slits are different. This is sufficient to bring into focus the importance of the transverse coherence in those experiments and to show that the second order degree of visibility obtained had to be below 100% in the original experiments. *Equivalently*, it can be said that the idler photons from crystal 1 and from crystal 2, in those experiments, are not well represented by a unique annihilation operator. One could then wonder how to design an experiment to achieve a higher value

for the degree of visibility.

To circumvent some of the difficulties associated with a simultaneous consideration of the transverse and longitudinal coherence times, the idea of a cavity for the idler beam is proposed. Being designed to support an idler mode, no measurement, even in principle, could be performed on the photons inside the cavity without severely perturbing the cavity itself. In this sense the idler photons are coherent by definition and the cavity field can be properly represented by a unique annihilation operator.

As the phenomenon of induced coherence without stimulated emission is independent of the intensity of the idler beam inducing the coherence^[1], the degree of visibility for the interference existing between the signal beams should be independent of the cavity losses. The following calculation is in agreement with this expected property.

V.1 The Hamiltonian

The proposed setup to study the enhanced indistinguishability of the idler beams emitted by the two crystals is shown in Fig. 13, where the two crystals in the cavity are pumped by the same UV laser with large coherence length. The idler beam is within the cavity that is properly matched to its wavelength while the signal beams are emitted as traveling waves. The cavity loss is connected to the idler photons, due to the down-conversion beam divergence and to diffraction limitations, besides mirror losses. The cavity geometry will be supposed such that a mode will be established within the cavity with the wavevector \mathbf{k}_b^+ and annihilation

operator \hat{b}^\dagger . The stochastic loss will be considered under Markoffian conditions.

A peculiarity of the down-conversion luminescence is that the phase matching conditions $\hbar\omega_0 = \hbar\omega_a + \hbar\omega_b$ and $\hbar\mathbf{k}_0 = \hbar\mathbf{k}_a + \hbar\mathbf{k}_b^+$ imposes a spatial symmetry breaking in the propagation of the idler photons inside the cavity; the notation $\mathbf{k}_b^+ = \mathbf{k}_b$ will be adopted for the mode wavevector in this ring-like cavity.

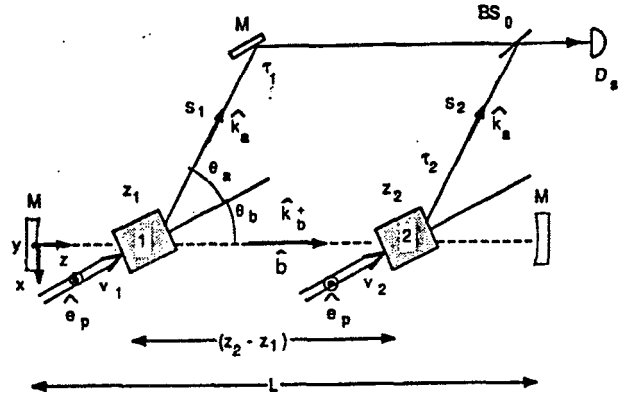


Figure 13. Basic outline of the proposed experiment. NL1 and NL2 are the two χ^2 nonlinear crystals pumped by the two classical field amplitudes v_1 and v_2 . Signal beams S_1 and S_2 are superposed on the beam splitter BS_0 and collected by detector D_s . The idler beam is emitted as a cavity mode with wavevector \mathbf{k}_b^+ . The center of the crystals are given by z_1 and z_2 along the z coordinate defined by the cavity optic axis. The laser beam polarization is vertical to the plane of the paper while the down-converted photons are polarized on that plane. The wavevectors for the signal beams are directed along $\hat{\mathbf{k}}_a$. τ_1 and τ_2 gives the propagation times from crystal 1 and from crystal 2 to BS_0 , respectively.

The Hamiltonian will be defined as

$$\begin{aligned} \hat{\mathcal{H}} = & \sum_{\omega_p} \hbar\omega_p \left(\hat{c}_1^\dagger(\omega_p)\hat{c}_1(\omega_p) + \hat{c}_2^\dagger(\omega_p)\hat{c}_2(\omega_p) \right) + \hat{V} \\ & + \sum_{\omega_{a_1}} \hbar\omega_{a_1} \hat{a}_1^\dagger(\omega_{a_1})\hat{a}_1(\omega_{a_1}) + \sum_{\omega_{a_2}} \hbar\omega_{a_2} \hat{a}_2^\dagger(\omega_{a_2})\hat{a}_2(\omega_{a_2}) + \hbar\omega_b \hat{b}^\dagger \hat{b} + \hat{b} \Gamma_b^\dagger + \Gamma_b \hat{b}^\dagger, \end{aligned} \quad (81)$$

where Γ_b specify a bath operator, \hat{c}_1 and \hat{c}_2 are annihilation operators for the pump photons, \hat{a}_1 and \hat{a}_2 are the annihilation operators for the signal photons and \hat{b} is the annihilation operator for the idler photons in the cavity. \hat{V} is the interaction term coupling the optical fields and the nonlinear crystals in a similar way as done in Ref. [1] but differing from it in the complete indistinguishability of the idler photons. The interaction operator \hat{V} is then given by

$$\hat{V} = \frac{\hat{b}^\dagger}{\Omega_c \sqrt{\Omega_b}} \left[\sum_{\mathbf{k}_a, s_a} \sum_{\mathbf{k}_p, s_p} I^*(\omega_a) I^*(\omega_b) I(\omega_p) e^{i(\omega_a + \omega_b - \omega_p)t} \hat{a}_1^\dagger(\mathbf{k}_a, s_a) \hat{c}_1(\mathbf{k}_p, s_p) \times \right.$$

$$\begin{aligned} & \times \mathcal{K}_1(\mathbf{k}) \int_{\text{ill. vol.}} d\mathbf{r}_1 e^{-i(\mathbf{k}_a + \mathbf{k}_b - \mathbf{k}_p) \cdot \mathbf{r}_1} \\ & + \sum_{\mathbf{k}'_a, s'_a} \sum_{\mathbf{k}'_p, s'_p} l^*(\omega'_a) l^*(\omega_b) l(\omega'_p) e^{i(\omega'_a + \omega_b - \omega'_p)t} \hat{a}_2^\dagger(\mathbf{k}'_a, s'_a) \hat{c}_2(\mathbf{k}'_p, s'_p) \\ & \times \mathcal{K}_2(\mathbf{k}') \int_{\text{ill. vol.}} d\mathbf{r}_2 e^{-i(\mathbf{k}'_a + \mathbf{k}_b - \mathbf{k}'_p) \cdot \mathbf{r}_2} \Big] + \text{H.c.} \end{aligned} \quad (82)$$

The \mathcal{K} 's are given by [1]

$$\mathcal{K}_l \equiv \left(\chi_{ijk}^{(2)} e^i_{\mathbf{k}_p, s_p} e^{*j}_{\mathbf{k}_a, s_a} e^{*k}_{\mathbf{k}_b, s_b} \right)_l \quad (83)$$

where $l = 1, 2$ and $\chi_{ijk}^{(2)}$ is the second order nonlinear susceptibility written in the principal axis of the crystal. The e 's are the unitary vectors for the electric fields associated with the modes and $\Omega = A(2\pi c/\delta\omega)$, where A is the cross section of the beam and $\delta\omega$ give the mode linewidths.

V.2 Time Evolution and the Fokker-Planck equation

The time evolution for the density matrix operator $\hat{\rho}$ in the interaction representation, considering the bath at low temperatures, will be given by^[34]

$$\frac{\partial \hat{\rho}}{\partial t} = -\frac{i}{\hbar} [\hat{V}, \hat{\rho}] + \gamma_b (2\hat{b}\hat{\rho}\hat{b}^\dagger - \hat{b}^\dagger\hat{b}\hat{\rho} - \hat{\rho}\hat{b}^\dagger\hat{b}). \quad (84)$$

The time evolution equation for $\hat{\rho}$ can be obtained and transformed into the Fokker-Planck equation for P , according to the positive-P representation^[34,35] where,

for example,

$$\hat{\rho}(t) = \int \frac{P(\{\alpha\}, \{\alpha^\dagger\}, t) |\{\alpha\}\rangle \langle \{\alpha^\dagger\}^*|}{\langle \{\alpha^\dagger\}^* | \{\alpha\} \rangle} d\{\alpha\} d\{\alpha^\dagger\} \quad (85)$$

and $\hat{a}_1, \hat{a}_2, \hat{b}$ transforms into $\{\mathbf{a}\} = \{\alpha_1, \alpha_2, \beta\}$ and $\{\alpha^\dagger\} = \{\alpha_1^\dagger, \alpha_2^\dagger, \beta^\dagger\}$ as the independent variables. Details of this calculation can be seen in Ref. [33]. It is interesting that these calculations do not restrict the number of photons to be 1 or 0, giving more generality to the results.

A very large number of terms is obtained from these equations, one for each allowed frequency, defining the wavepackets around each wavelength. A simplification was introduced to achieve the maximum degree of visibility of the interference between the two signal beams on the beam splitter BS_0 , and not to obtain information about the coherence length of each signal beam: The decay of the degree of visibility as the paths of the two signal beams are made unequal has no immediate interest and, in this case, the large number of terms obtained is largely reduced with the substitution $\alpha(\omega_a) \rightarrow \alpha(\omega_{0a})$. The resulting Fokker-Planck equation is

$$\begin{aligned} \frac{\partial P}{\partial t} = & \left[-\frac{\partial}{\partial \beta} (g_1 \alpha_1^\dagger + g_2 \alpha_2^\dagger - \gamma_b \beta) - \frac{\partial}{\partial \beta^\dagger} (g_1^* \alpha_1 + g_2^* \alpha_2 - \gamma_b \beta^\dagger) \right. \\ & - \frac{\partial}{\partial \alpha_1} g_1 \beta^\dagger - \frac{\partial}{\partial \alpha_1^\dagger} g_1^* \beta - \frac{\partial}{\partial \alpha_2} g_2 \beta^\dagger - \frac{\partial}{\partial \alpha_2^\dagger} g_2^* \beta \\ & \left. + \frac{\partial^2}{\partial \alpha_1 \partial \beta} g_1 + \frac{\partial^2}{\partial \alpha_1^\dagger \partial \beta^\dagger} g_1^* + \frac{\partial^2}{\partial \alpha_2 \partial \beta} g_2 + \frac{\partial^2}{\partial \alpha_2^\dagger \partial \beta^\dagger} g_2^* \right] P, \end{aligned} \quad (86)$$

where

$$|g_j| \cong \frac{|\eta_j| |v_{0j}| \sin(\frac{\Delta\omega_a}{2c} z_j \hat{\mathbf{k}}_a \cdot \hat{\mathbf{z}})}{\sqrt{2\pi} (\frac{\Delta\omega_a}{2c} z_j \hat{\mathbf{k}}_a \cdot \hat{\mathbf{z}})}, \quad (87)$$

and

$$\varphi_j = \varphi_{\eta_j} + \varphi_{v_j} + \Phi(\phi_j) - k_b z_j - \frac{\omega_{0a}}{c} z_j \hat{\mathbf{k}}_a \cdot \hat{\mathbf{z}} - \frac{\pi}{2}, \quad (88)$$

$\Delta\omega_a (\cong \Delta\omega_p)$ is the frequency spread of the signal pho-

tons and Φ is the phase of ϕ .

This equation contains the necessary minimum ingredients to investigate some of the basic properties of the correlations between the signal electric fields as depicted in Fig. 1. While in this simplification α_j represents the field amplitudes at the frequencies ω_{0a} , the function g_j contains information on the frequency spread $\Delta\omega_a$ around ω_{0a} .

Due to its inherent character of a diffusion equation for a single-mode, results arising from its solutions cannot be arbitrarily taken under risk of violating the con-

ditions determining stochastic processes. The limits of $y = 0$ and $y \rightarrow \infty$ shows, respectively, a ballistic regime not covered by stochastic equations and the absence of the cavity. The absence of the cavity leads to the continuum of modes existing in the free down-conversion luminescence. This continuum is not achievable from our single mode theory.

V.3 Second-order Degree of Visibility

The electric field associated with each signal beam superposed on the beam splitter BS_0 will be given by

$$E_j(t) = \sqrt{\frac{\delta\omega_a}{2\pi}} \alpha_j(t) e^{i(\mathbf{k}_j \cdot \mathbf{r}_j - \omega_{a_j} t)} = \sqrt{\frac{\delta\omega_a}{2\pi}} \alpha_j(t) e^{i\omega_{a_j} \left[(\tau_j - t) + \frac{z_j}{c} \hat{\mathbf{k}}_a \cdot \hat{\mathbf{z}} \right]} \quad (89)$$

where $j = 1, 2$. The second order correlation function $\mathcal{G}_s^{(2)}$ measured by detector D_s is

$$\mathcal{G}_s^{(2)}(t) = \left\langle \left(\frac{E_1^*(t) - iE_2^*(t)}{\sqrt{2}} \right) \left(\frac{E_1(t) + iE_2(t)}{\sqrt{2}} \right) \right\rangle, \quad (90)$$

The solutions for the correlation functions $\langle \alpha_j^*(t) \alpha_j(t+\tau) \rangle$ were obtained in Ref. [25]. From them it is straightforward to obtain the correlation for the electric fields

$$\begin{aligned} \frac{4\pi}{\delta\omega_a} \mathcal{G}_s^{(2)}(t; \tau_1 - \tau_2) &= \frac{1 - e^{-2t|g_1|\sin\psi_1}}{2\sin\psi_1} + \frac{1 - e^{-2t|g_2|\sin\psi_2}}{2\sin\psi_2} \\ &+ 2\mathcal{M} \left[\sin\zeta - e^{-t(|g_1|\sin\psi_1 + |g_2|\sin\psi_2)} \sin \left(\zeta + t(|g_1|\cos\psi_1 - |g_2|\cos\psi_2) \right) \right], \end{aligned} \quad (91)$$

where

$$\psi_j = - \left(k_b + \frac{\omega_{0a}}{c} \hat{\mathbf{k}}_a \cdot \hat{\mathbf{z}} \right) z_j, \quad (92)$$

$$\mathcal{M} = \sqrt{\frac{|g_1||g_2|}{|g_1|^2 + |g_2|^2 - 2|g_1||g_2|(\cos\psi_1\cos\psi_2 - \sin\psi_1\sin\psi_2)}}, \quad (93)$$

and

$$\zeta = \left[\omega_{0a}(\tau_1 - \tau_2) + k_b(z_2 - z_1) + \arctan \left(\frac{|g_1|\cos\psi_1 - |g_2|\cos\psi_2}{|g_1|\sin\psi_1 + |g_2|\sin\psi_2} \right) \right]. \quad (94)$$

The degree of visibility $\vartheta^{(2)}$ is defined as

$$\vartheta^{(2)} \equiv \frac{\mathcal{G}_s^{(2)}{}_{max} - \mathcal{G}_s^{(2)}{}_{min}}{\mathcal{G}_s^{(2)}{}_{max} + \mathcal{G}_s^{(2)}{}_{min}} \quad (95)$$

that in the stationary condition ($t \rightarrow \infty$, $\sin\psi_j > 0$) gives

$$\vartheta^{(2)}{}_{stat} = \frac{4\sin\psi_1\sin\psi_2}{\sin\psi_1 + \sin\psi_2} \mathcal{M}. \quad (96)$$

The maximum value for $\vartheta^{(2)}{}_{stat}$ is 1.

This interference presents interesting peculiarities,

as independence of the loss parameter γ_b and a strong dependence on the position of the crystals inside the cavity. This independence from the idler loss emphasizes that the phenomenon of "induced coherence without stimulated emission" depends exclusively on *geometric* conditions.

The second order correlation function for the superposed signal fields obtained shows the dependence on all relevant quantities. The maximum value expected for the second order visibility is $\vartheta^{(2)} \simeq 1$.

A simplified but equivalent experimental scheme was designed to show the predicted visibility increase that should be associated with this more perfect indistinguishability. Fig. 14 shows the experimental set-up that was suggested by the experiment shown in Ref. [36]. In that experiment a single-mode laser was used such that interference fringes could be generated on the crystal between the direct pump laser and its reflection. In this new experiment a multi-mode beam ought to be used avoiding this interference between pump beams.

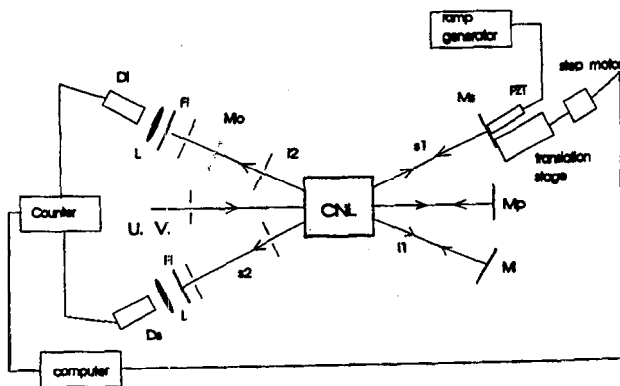


Figure 14. Setup with only one crystal, equivalent to the setup shown in Fig. 13.

In this way, at least in first order, the downconversion modes generated by the pump beam and by the reflected one will not be affected by pump interferences. The situation is completely analogous to Fig. 13; the downconverted beams produced by the incoming pump laser may be seen as produced by "crystal 1", while the ones produced by the reflected pump would be produced by "crystal 2". A complete indistinguishability of idler photons generated by "crystal 1" and "2" is then expected. Interference fringes could be generated, for example, by PZT translation of the signal mirror M_s .

Preliminary results were obtained before the cavity was set with coincidence fringes between D_s and D_i and typical counts of 100 cps or single counts of order 2×10^4 . Interference filters of bandwidth $\sim 100 \text{ \AA}$ were used. However, with the cavity in place to define a mode, its bandwidth would be much narrower than the interference filter used, $\sim 10^3$ or $\sim 10^4$ times narrower. In order to perform measurements upon the signal beam corresponding to a mode conjugated to the one within the cavity, a similar narrow filter have to be used in the signal beam with a severe attenuation of the selected signal, of the same order as the reduction

in bandwidth. Unfortunately, this brings the signal to the existent detector noise level. In order to achieve success in these measurements, the system has to be improved: all the coatings used on the crystals have to be optimized, a cavity matched to the signal wavelength should be used. These conditions are not available presently at our laboratory.

V. Young fringes and non-localized control of Visibility. Quantum Images.

A. Controlling the degree of visibility of Young's fringes with photon coincidence measurements

It is a known fact that the Young's double-slit experiment done with an extended incoherent quasi-monochromatic light source generates an interference pattern when one dimension of the coherence area, the dimension corresponding to the direction of the ray vector joining the slits, is larger than the separation between slits. This subject has been discussed in detail by Born and Wolf^[37] in their presentation of the Van Cittert-Zernike theorem. Coherence area measurements are widely used in applications where light is produced by an extended source. From the knowledge of this area, we can estimate the size of the source needed in interference and diffraction experiments.

Along this classical idea, the coherence area was measured in a Young's experiment using parametric down conversion light generated by a non-linear crystal^[38]. The experiment was done with only one of the beams from the parametric downconversion and the intensity distribution of the transmitted light, measured for several source-slits distances. At the point where the interference fringes pattern disappear, one dimension of the coherence area is equal to the separation between the slits, giving the way to determine the coherence area. For even shorter source-slits distances, the interference fringes pattern disappear as expected for extended quasi-monochromatic incoherent sources^[37].

Another recent experimental work^[39] answered the question whether is it possible to detect the interference from an extended incoherent source with Young's slits when the source-slits distance is such that all dimen-

sions of the coherence area of the incident light beam are smaller than the distance between the slits. It was shown that, under that condition, interference fringes can be obtained with a controlled degree of visibility by means of coincidence measurements between conjugated beams of the downconversion luminescence. This was the *first* experiment of two particle interferometry utilizing Young slits (for a fine review on multiparticle interferometry, see Ref. [40]).

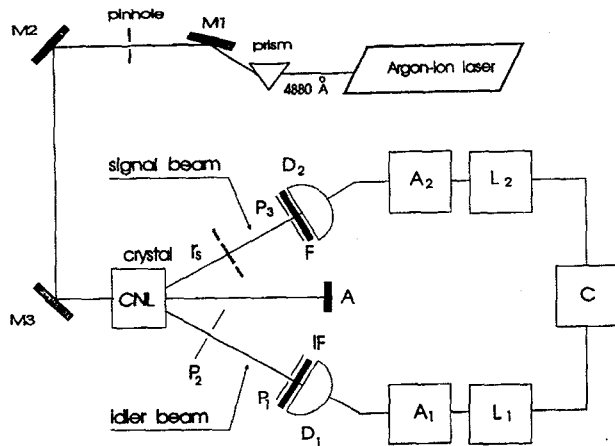


Figure 15. Schematic diagram of the experimental setup for Young's double slit experiment. M_1 and M_2 are mirrors, P_1 , P_2 and P_3 are pinholes, D_1 and D_2 are photomultipliers, IF is an interference filter, F is an absorption filter, A is a beam stop, A_1 and A_2 are pulse formatting devices, L_1 and L_2 are delay lines, C is the coincidence detection system, and r_s is the distance between source and slits.

See Fig. 15. Parametric downconversion luminescence is produced by a $LiIO_3$ nonlinear crystal when it is pumped by a 100 mW argon-ion laser emitting at 3511 Å. Two beams with wavelengths around 7887 Å (signal) and 6328 Å (idler) are chosen by setting the detectors at angles 32° (signal) and 25° (idler) with respect to the pump beam direction and by using filters with bandwidth 400 Å and 100 Å respectively, at the photomultipliers tube entrances. Pinholes mounted in 2-D stages are used for defining the signal and idler beams directions ($\phi(P_1)=0.6$ mm, $\phi(P_2)=2.0$ mm and $\phi(P_3)=0.5$ mm). The width of each slit and the distance between them, measured with a microscope, are 80 μm and 90 μm respectively. The slits are aligned *along* the plane of the pump laser and the down-converted beams. Interference fringes are detected by means of coincidence measurements between the idler beam and the transmitted signal beam through the Young's slits. The detector at the idler beam is kept

fixed while the signal beam detector is scanned in the direction perpendicular to the larger slits dimension.

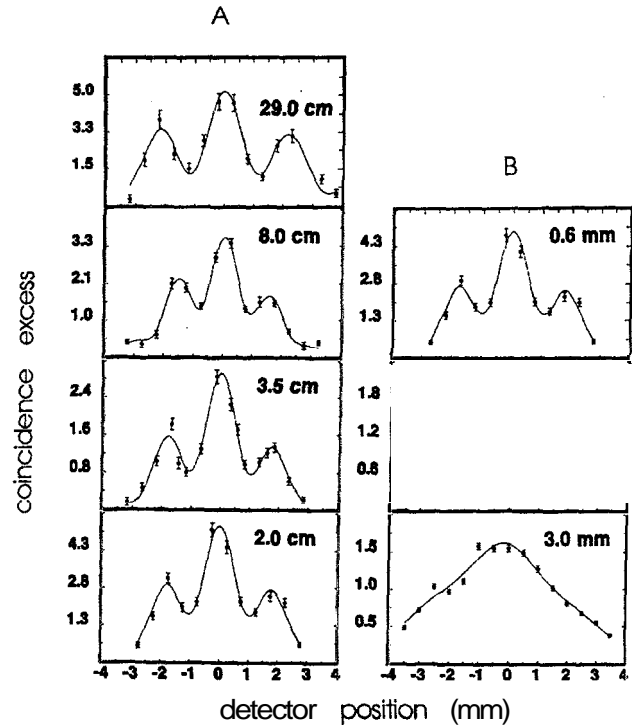


Figure 16. A: shows experimental points showing the coincident excess as function of the detector position, and fittings. The distance between source and slits and visibilities are $r_s = 295$ mm and $\mu_{12} = 0.57 \pm 0.06$; $r_s = 80$ mm and $\mu_{12} = 0.44 \pm 0.03$; $r_s = 35$ mm and $\mu_{12} = 0.52 \pm 0.05$; $r_s = 20$ mm and $\mu_{12} = 0.46 \pm 0.06$. The pinhole P_1 diameter is $\phi(P_1) = 0.6$ mm. B: shows coincidence interference patterns for different diameters of pinhole P_1 . Source to slits distance is $r_s = 20$ mm. The pinhole P_1 diameters and visibilities are $\phi(P_1) = 0.6$ mm and $\mu_{12} = 0.46 \pm 0.06$, $\phi(P_1) = 1.8$ mm and $\mu_{12} = 0.13 \pm 0.04$, and $\phi(P_1) = 3.0$ mm and $\mu_{12} = 0.09 \pm 0.04$.

Fringes interference patterns were detected for several source to slit distances, even for distances as short as 20 mm that was the minimum possible distance for the setup. On the other hand, for a fixed distance between source and idler beam detector, it was observed that the interference pattern is dependent on the idler pinhole diameter in front of the detector.

Due to the lack of a theory to fit the experimental points and the observation that the shape of the coincidence patterns, Fig. 16, were quite similar to the ones obtained in a first order coherence experiment, the following phenomenological function was used to fit the experimental points

$$E(Q) = E_0(Q)[1 + \mu_E \cos(\alpha_E + \delta)], \quad (97)$$

where $E(Q)$ is the coincidence excess with the signal beam detector at the point (Q), μ_E is an adjustable parameter, δ is the path difference between fields originating at slit 1 and slit 2, α_E is also adjustable and $E_0(Q)$ is given by

$$E_0(Q) = E_{0N} \left[\frac{\sin(k_s p x)}{(k_s p x)} \right]^2, \quad (98)$$

where E_{0N} is a normalization factor, x is the variable coordinate of the point (Q) and p is connected with the slit width.

The coincidence patterns for four distances between source and slits and fittings are shown in Fig. 16A. They were obtained with a sampling time of 1800 s in each point and a resolution time of 10 ns for the coincidence~.

For the closest source to slit distance, coincidence interference patterns were obtained with the diameter of the pinhole P_1 increased from $\phi(P_1) = 0.6$ mm to $\phi(P_1) = 1.8$ mm and to $\phi(P_1) = 3.0$ mm. The patterns and fittings are shown in Fig. 16B.

Coincidence source profiles were obtained by making the same kind of measurements without slits. For the pinhole P_1 with diameter $\phi(P_1) = 0.6$ mm these profiles are shown in Fig. 17 for three distances r_d between source and detector. The sampling time was reduced to 300 s, because of the signal increase without slits. Fitting these profiles with a Gaussian function, information about the effective size of the source for coincident experiments is obtained.

The function chosen to fit the experimental points is analogous to the expression for the intensity interference patterns in first order coherence experiments. This analogy can lead us to interesting conclusions about the measurements.

The parameter μ_E in Eq. (97) is the counterpart of the Young's fringes visibility in a first order coherence experiment. We compare in Table 1 the coincidence visibility μ_E obtained by the fittings, with the prediction for the visibility μ_{12} in a first order coherence experiment^[37,38] with the same parameters of the second order coherence experiment performed. While the fittings are rather good, the coincidence visibility μ_E is always larger than the first order prediction of μ_{12} , even for short distances between source and slits. Note that those values for μ_E cannot be explained even by a small effective source size measured with coinci-

dente detection, because the measured size, $\sigma_0 = 1.67 \pm 0.23$ mm, is not small. (See Fig. 17).

TABLE I. Comparison between the degree of visibility μ_{12} given by a first order coherence theory and the experimentally obtained μ_E through coincidence measurements.

Source-slits distance (mm)	Visibilities	
	μ_E	μ_{12}
295	0.57 ± 0.06	0.23
80	0.44 ± 0.03	~ 0
35	0.52 ± 0.05	~ 0
20	0.46 ± 0.06	~ 0

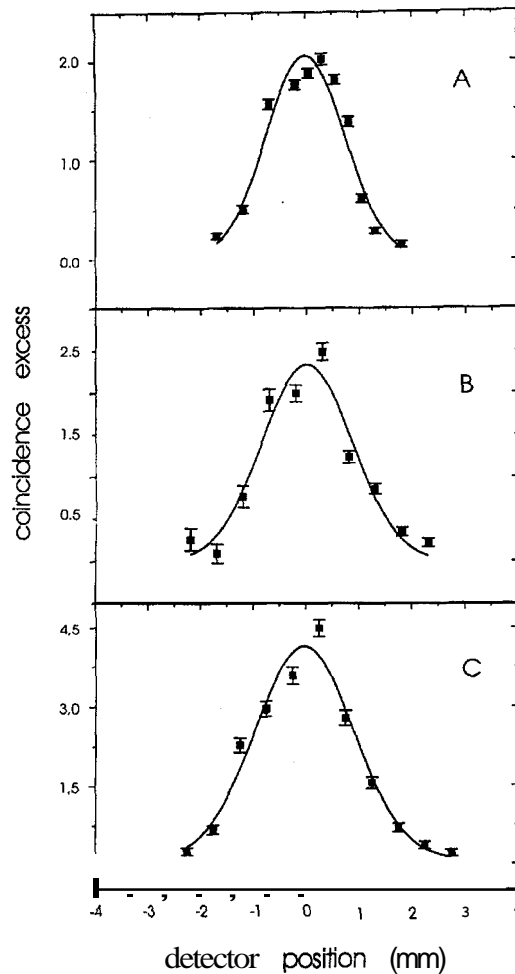


Figure 17. coincidence source profiles and fittings. The P_1 diameter is $\phi(P_1) = 0.6$ mm. The distances r_d between source and signal beam detector and the Gaussians FWHM are $r_d = 130$ mm and $\sigma = 1.82 \pm 0.16$ mm in (A), $r_d = 250$ mm and $\sigma = 1.92 \pm 0.18$ mm in (B), and $r_d = 430$ mm and $\sigma = 2.13 \pm 0.15$ mm in (C). The projected width on the source position is $\sigma_0 = 1.67 \pm 0.23$ mm.

It is clearly shown that it is not possible to use the first order coherence theory to fit the second order co-

herence experiment results, even noting that the patterns produced by the two kind of experiments are very alike. However, the profiles shown in Fig. 16, in which the *coincidence visibility* μ_E is decreased by increasing the idler beam pinhole (P_1) diameter, indicate how to use the first order coherence theory to understand qualitatively the behavior of the coincidence patterns.

An extended incoherent source produces a superposition of interference patterns after the Young slits, due to each light mode present in the radiation field. The mode frequency can be defined by a narrow width filter ($\sim 100 \text{ \AA}$) in the slits beam and a certain range of wavevectors \mathbf{k} , is accepted through the slits. As the detection of the interference patterns is done by a coincidence scheme, only photons which have a twin on the conjugated beam will be detected within the photons of the superposed patterns.

When the idler beam detector pinhole (P_1) diameter is varied, as in Fig. 16, idler beam wavevectors \mathbf{k}_i are selected. As the momentum conservation implies in a strong correlation between the twin photons wavevectors, the signal beam wavevectors \mathbf{k}_s are also selected within the collected signal light by the coincidence detection. In other terms, only some interference patterns are selected, resulting in the control of the fringes visibility by means of the idler beam pinhole diameter (P_1). In this way, interference can always be detected, even if the slits are very close to the source.

Of course a second order coherence theory must be developed to *quantitatively* show the complete dependence of the coincidence patterns on the system param-

eters, but this qualitative explanation based on first order coherence concepts is useful in the understanding of this interesting selection mechanism. This mechanism explaining the *selection* of first order patterns within the superposed patterns, justifies the form adopted for the coincidence excess given by Eq. (1).

These measurements show interference fringes with a reasonable contrast, even when the light transmitted through the slits is incoherent in the sense that all dimensions of the first order coherence area are smaller than the distance between slits. This is possible if we use the coincidence detection scheme with the beam without slits being detected under conditions that permit the selection of the *coherent* photons. It was then demonstrated that the degree of Young's fringe visibility can be controlled through the conjugated idler beam. This is a simple demonstration of two particle interferometry.

Analogously as done in the classical Van-Cittert Zernike theorem for the first order correlation function, the results shown in this work suggest that *entangled coherence areas* could be *simultaneously* specified for the conjugated *signal* and *idler* beams through the fourth order correlation function.

Fourth-order correlation function; Quantum Images.

The explanation of that entanglement between coherence areas can be done quantum-mechanically through a direct calculation of the fourth order correlation function¹⁸

$$\mathcal{G}^{(4)} = \langle \psi(t) | \hat{E}_s^{(-)}(\mathbf{r}_s, t) \hat{E}_i^{(-)}(\mathbf{r}_i, t + \tau) \hat{E}_i^{(+)}(\mathbf{r}_i, t + \tau) \hat{E}_s^{(+)}(\mathbf{r}_s, t) | \psi(t) \rangle, \quad (99)$$

where the wavefunction $|\psi(t)\rangle$ is given in Eq. (37), \mathbf{r} , and \mathbf{r}_i specifies the positions of the signal and idler detectors, respectively, and the electric fields \hat{E}_s and \hat{E}_i refers to signal and idler fields at given positions. This is a special case of a four-point $\mathcal{G}^{(4)}$ that could also be used instead to this calculation.

In the experiment performed, $\hat{E}_s^{(+)}(\mathbf{r}_s, t)$ is the sum of the fields incident on the signal detector from the two slits placed in the signal beam path. Writing these fields as $\hat{E}_j^{(\pm)}(\mathbf{r}_{sj}, t_j)$ the correlation function $\mathcal{G}^{(4)}$ is

$$\begin{aligned} \mathcal{G}^{(4)} = & \langle \hat{E}_1^{(-)} \hat{E}_1^{(+)} \hat{E}_i^{(-)} \hat{E}_i^{(+)} \rangle + \langle \hat{E}_1^{(-)} \hat{E}_2^{(+)} \hat{E}_i^{(-)} \hat{E}_i^{(+)} \rangle + \\ & + \langle \hat{E}_2^{(-)} \hat{E}_1^{(+)} \hat{E}_i^{(-)} \hat{E}_i^{(+)} \rangle + \langle \hat{E}_2^{(-)} \hat{E}_2^{(+)} \hat{E}_i^{(-)} \hat{E}_i^{(+)} \rangle. \end{aligned} \quad (100)$$

¹⁸Sometimes the name second-order correlation function is used, with the notation $G^{(2,2)}$, instead of fourth-order correlation function. Of course, the superscripts (2, 2) indicate four fields in the averaging process.

The entanglement between signal and idler photons is produced at the crystal source and all spatial (angular) information on the far radiation field is contained in the double point spectral density function $\gamma(\mathbf{r}_s, \mathbf{r}_i; \mathbf{k}_s, \mathbf{k}_i)$, defined by

$$\gamma(\mathbf{r}, \mathbf{r}_i; \mathbf{k}_s, \mathbf{k}_i) \equiv \int \int_{\text{radiation field}} d\Omega_s d\Omega_i \phi(\mathbf{k}_s, \mathbf{k}_i; \mathbf{k}_p) e^{i\mathbf{k}_s \cdot \mathbf{r}} e^{i\mathbf{k}_i \cdot \mathbf{r}_i}, \quad (101)$$

where $d\Omega_s = d\phi_s d\theta_s \sin\theta_s$ and $d\Omega_i = d\phi_i d\theta_i \sin\theta_i$ are solid angles for the signal and idler fields around the origin at the crystal, \mathbf{k}_s and \mathbf{k}_i are the signal and idler wavevectors. The spectral density function $\phi(k_s \hat{k}_s, k_i \hat{k}_i; \hat{k}_p)$ for the PDC

$$\phi = j_0 \left[(k_s \sin\theta_s \cos\phi_s + k_i \sin\theta_i \cos\phi_i) \frac{l_x}{2} \right] \times j_0 \left[(k_s \sin\theta_s \sin\phi_s + k_i \sin\theta_i \sin\phi_i) \frac{l_y}{2} \right] \times j_0 \left[(k_s \cos\theta_s + k_i \cos\theta_i - k_p) \frac{l_z}{2} \right], \quad (102)$$

where l_x, l_y and l_z are the crystal lengths along the x, y and z axis and j_0 is the spherical Bessel function of the first kind.

The visibility $\mathcal{V}^{(4)}$ can be obtained, as usual, from the maximum and minimum of $\mathcal{G}^{(4)}$, as $\mathcal{V}^{(4)} = (\mathcal{G}_{\max}^{(4)} - \mathcal{G}_{\min}^{(4)}) / (\mathcal{G}_{\max}^{(4)} + \mathcal{G}_{\min}^{(4)})$.

The use of a finite area for the idler pinhole implies an average over $\mathcal{V}^{(4)}$ that is "point" defined. Within the same approach, the signal slits can be treated as "point" slits. An average over pinhole and slits area should give a decreased visibility.

While the above "recipe" is very simple, the practical calculation is quite difficulty due to the complexity of the ϕ function. No exact solution has been presented up to now¹⁹, although simplified attempts have been presented. Ref. [41] shows a calculation of the "coupled" visibility, treating ϕ as a constant. Fig. 18 shows the visibility obtained in that paper.

Although this is still an open problem, the expected coupling between the signal and idler can be seen as an aspect of an extended Van Cittert-Zernike theorem for the fourth-order correlation function of the PDC.

These are indications of possible applications of this concept in the optical communication field, because any non-localized control of interferences may find practical utilization. Indeed, if one understands the fringe pattern as an *object* detected in the signal beam after the slits, one should expect that a conjugate object, or image, should appear in the idler beam, because to every

signal point probed a conjugated idler point should exist - even if the object is an "interference" pattern.

This expected image should be revealed in coincident measurements or, fourth order correlation functions, but not in the intensity pattern that may be even constant over the probed region. The name *quantum images* has been coined to patterns (information) seen in the spatial correlation functions, instead of being seen in intensity distributions. While it has been applied mainly to quantum images formed by OPO's, the basic idea is the same.

Quite remarkably, the fringe pattern created by a double slit in the signal beam was detected as an *image* in the idler beam, where no slits exist^[42]. A setup following the one in Ref. [39] was used.

In the same way as transverse correlations shows the conjugate "object-image" patterns, an experiment could be set to show longitudinal "images": For example, the experiment presented in Sec. II could be done taking the detector after the cavity as the "start" detector and the detector at the other side could be translated along the beam propagation direction revealing "ghost" peaks at positions $l_0 = 0, l_1 = 2c\tau_1$, and so on.

These facts, and the potentiality for practical applications, emphasizes the need for a broader study of this problem.

¹⁹A solution quite recently found by the author was submitted to publication in *Phys. Rev. A* (Nov. 1995), after the acceptance of this paper.

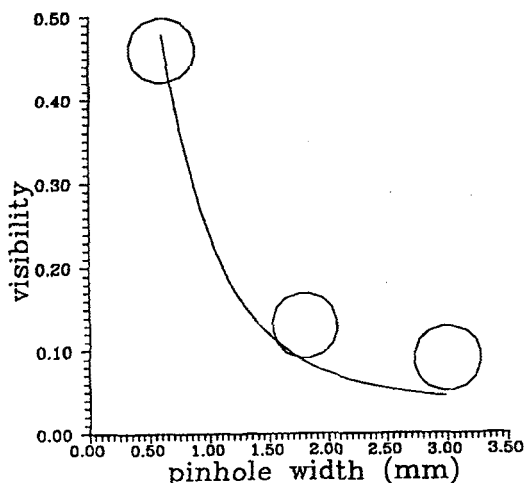


Figure 18. Fourth order visibility in function of the idler pinhole diameter. The Young slits are placed on the signal beam path.

B. Control of Young's fringes by stimulated down-conversion

Another form of visibility control was explored in Ref. [43] utilizing stimulated emission. It was shown that the degree of visibility of the interference fringes produced by a *signal* beam transmitted through a double-slit, can be also controlled by aligning an auxiliary laser with the *idler* beam, with the same wavelength and varying its intensity. In this case, the degree of coherence of the source is varied directly by the inducing laser intensity without performing any measurements on the *idler* beam.

A 3 mW He-Ne laser, aligned with the 6328 Å downconverted beam, stimulates the 7887 Å (*signal*)

- 6328 Å (*idler*) conjugate pair emission. (See Fig. 19).

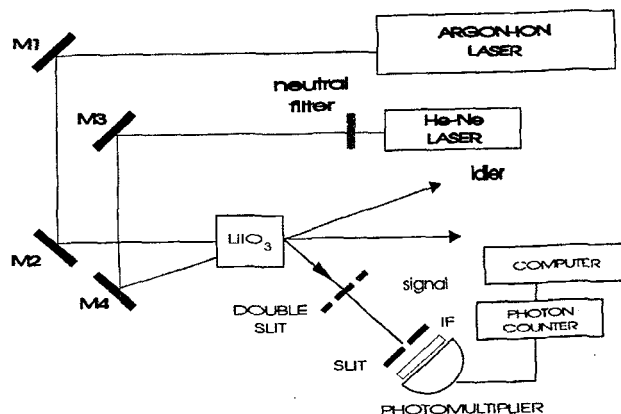


Figure 19. Schematic diagram of the experimental setup for the stimulated Young's double-slit experiment. M₁, M₂, M₃, M₄ are mirrors, IF is an interference filter and NF is a neutral filter.

The double-slit is positioned at 8 cm from the crystal in the path of the 7887 Å *signal* beam. The interference pattern distribution is measured with a photomultiplier (PMT), 35 cm far from the slits, mounted on a Z-axis translation stage. The scans are performed with a 300 μm slit at the PMT entrance. An interference filter with 100 Å bandwidth and centered on 7887Å, placed at the PMT entrance, assures that the detected light is almost monochromatic. The inducing laser intensity is controlled by neutral filters placed before the crystal. (See interference fringes in Fig. 20).

To explain the experimental results a simple formula is obtained as follows. The intensity distribution of the interference pattern for a typical Young's double slit experiment is given by Ref. [37] as

$$I(Q) = I_1(Q) + I_2(Q) + \sqrt{I_1(Q)I_2(Q)} |\mu_{12}| \cos[\alpha_{12}(\tau) - \delta], \tag{103}$$

where $I_1(Q)$ and $I_2(Q)$ are the single slit diffraction patterns for each slit, δ is the phase path difference between each slit and the observation point Q, μ_{12} is the normalized mutual intensity and α_{12} is its phase.

The modulus of the normalized mutual intensity gives us the visibility of the interference fringes, μ_{12} is defined as

$$\mu_{12} = \frac{\langle \mathbf{E}^*(\mathbf{r}_1) \cdot \mathbf{E}(\mathbf{r}_2) \rangle}{\sqrt{\langle \mathbf{E}^*(\mathbf{r}_1) \cdot \mathbf{E}(\mathbf{r}_1) \rangle \langle \mathbf{E}^*(\mathbf{r}_2) \cdot \mathbf{E}(\mathbf{r}_2) \rangle}}, \tag{104}$$

where \mathbf{E} is the electric field and $\mathbf{r}_1, \mathbf{r}_2$ specify the position of the slits.

The light produced in the stimulated downconversion is a superposition of a coherent and an incoherent field,

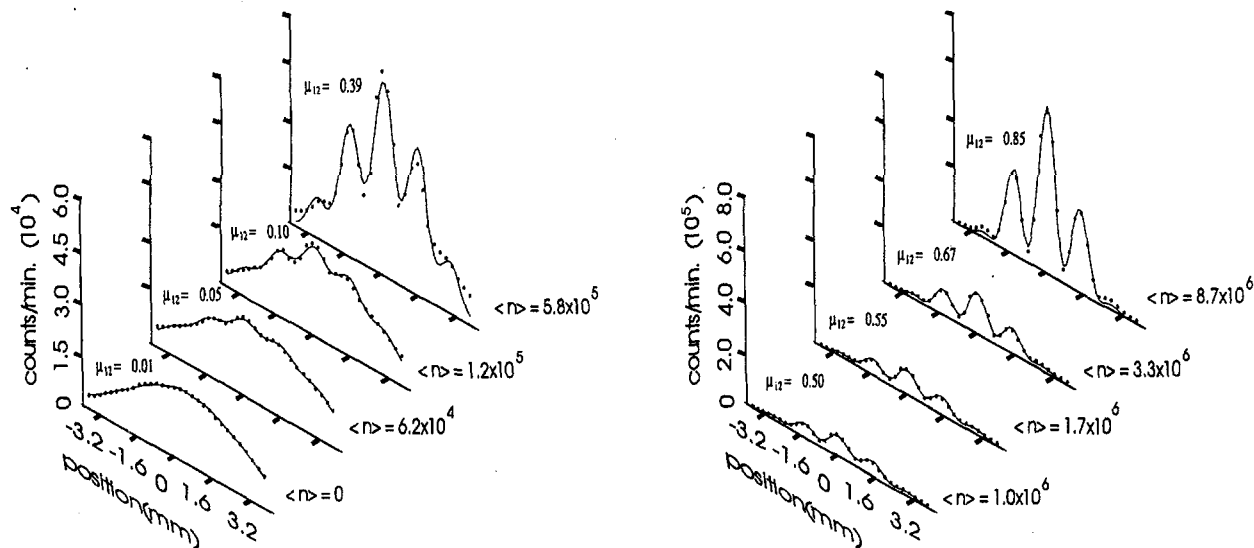


Figure 20. Experimental points showing the intensity patterns as a function of the detector position (circles), and fittings (line). Errors bars are the same size as the circles.

$$\mathbf{E}(\mathbf{r}) = \mathbf{E}_c(\mathbf{r}) + \mathbf{E}_i(\mathbf{r}). \tag{105}$$

With this sum of fields, the expression for the mutual intensity gives

$$\begin{aligned} \langle \mathbf{E}^*(\mathbf{r}_1) \cdot \mathbf{E}(\mathbf{r}_2) \rangle = & \langle \mathbf{E}_c^*(\mathbf{r}_1) \cdot \mathbf{E}_c(\mathbf{r}_2) \rangle + \langle \mathbf{E}_i^*(\mathbf{r}_1) \cdot \mathbf{E}_i(\mathbf{r}_2) \rangle + \\ & \langle \mathbf{E}_c^*(\mathbf{r}_1) \cdot \mathbf{E}_i(\mathbf{r}_2) \rangle + \langle \mathbf{E}_i^*(\mathbf{r}_1) \cdot \mathbf{E}_c(\mathbf{r}_2) \rangle. \end{aligned} \tag{106}$$

The correlation functions with \mathbf{E} , and \mathbf{E}_i will sum up to zero because the incoherent field phase is random and the coherent field phase is not. Thus, only the terms with the same kind of fields will give a non zero contribution. The expression for the normalized mutual intensity will be

$$\mu_{12} = \frac{\mu_i I_i + \mu_c I_c}{I_i + I_c}, \tag{107}$$

where $\mu_i = \langle \mathbf{E}_i^*(\mathbf{r}_1) \cdot \mathbf{E}_i(\mathbf{r}_2) \rangle / I_i$, is the normalized

mutual intensity for the incoherent field, $\mu_c = \langle \mathbf{E}_c^*(\mathbf{r}_1) \cdot \mathbf{E}_c(\mathbf{r}_2) \rangle / I_c$, is the normalized mutual intensity for the coherent field, $I_i = \langle \mathbf{E}_i^*(\mathbf{r}_1) \cdot \mathbf{E}_i(\mathbf{r}_1) \rangle = \langle \mathbf{E}_i^*(\mathbf{r}_2) \cdot \mathbf{E}_i(\mathbf{r}_2) \rangle$ is the intensity of the incoherent field at the slits and $I_c = \langle \mathbf{E}_c^*(\mathbf{r}_1) \cdot \mathbf{E}_c(\mathbf{r}_1) \rangle = \langle \mathbf{E}_c^*(\mathbf{r}_2) \cdot \mathbf{E}_c(\mathbf{r}_2) \rangle$ is the analog for the coherent field. The intensities at the two slits were considered equal, because the distance between them ($90 \mu\text{m}$) is much smaller than the distance between source and slits (8 cm).

Using the *average occupation number per mode*^[1], that can be expressed in terms of ratio of the coherent to incoherent intensities $\mathcal{N} = I_c/I_i$, a final form for the normalized mutual intensity is obtained

$$\mu_{12} = \frac{\mu_i + \mu_c \mathcal{N}}{\mathcal{N} + 1}. \quad (108)$$

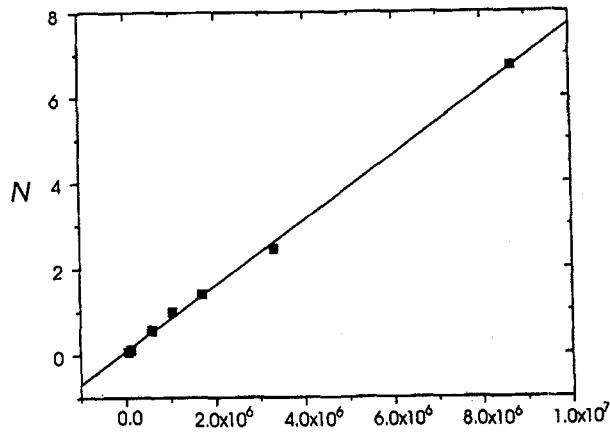


Figure 21. Experimental occupation numbers \mathcal{N} as a function of $\langle n \rangle$ the inducing laser mean photon number. A fit to Eq.(8) gives $\beta = (7.74 \pm 0.11) \times 10^{-7}$. Error bars are the same size as the symbols.

The interference patterns shown in Fig. 20 were obtained by varying the inducing (He-Ne) laser intensity (I_i). The slits were placed at a distance from the light source such that the coherence area for the spontaneous emitted light is smaller than the distance between the slits^[38]. Thus the visibility for $I_i = 0$, that corresponds to $\mathcal{N}=0$, is nearly zero. Clearly, the increase of I_i produces interference patterns with increasing visibilities. In this way, a control of the spatial coherence of the signal beam can be achieved by varying the intensity of the laser beam aligned with the idler beam. The visibilities are obtained from the interference patterns by a fit to Eq. (103) and considering the finite size of the detector.

To compare theory and measurements, the *average occupation number per mode*

$\mathcal{N} = (2\pi)^2 |\phi(\omega_p, \omega_s, \omega_i; \mathbf{K}_p, \mathbf{K}_s, \mathbf{K}_i)|^2 |W|^2$ [1] should be used. In this expression, $\phi(\omega_p, \omega_s, \omega_i; \mathbf{K}_p, \mathbf{K}_s, \mathbf{K}_i)$ is the spectral density function for the downconversion and $|W|^2$ is the photon rate of the inducing laser. The indexes p,s and i refer to pump, signal and idler respectively. This calculation does not take into account the coupling efficiency between laser and downconversion

field modes. However, the function $\mathcal{N} = \beta \langle n \rangle$ can fit measured values of \mathcal{N} as a function of the inducing laser mean photon number ($\langle n \rangle$), that is proportional to $|W|^2$. ($\langle n \rangle$ is the number of photons within one coherence volume and it was obtained by measuring the inducing laser power and its coherence time and multiplying the laser power in photons per unit of time by the coherence time. β is the coupling parameter, obtained from the plot of \mathcal{N} versus $\langle n \rangle$. This is shown in Fig. 21.

The measured visibilities are compared with the theory given by Eq. (108) in Fig. 22, showing a reasonable agreement. When the stimulated downconversion is produced, a light beam which is partially coherent in the spatial sense is obtained, because it is a superposition of coherent and incoherent light. Since the coherent to incoherent light intensity ratio in the signal beam is dependent on the inducing laser intensity, the spatial coherence in the signal beam can be controlled through the laser aligned with the idler beam. The degree of visibility of the patterns is a measure of the correlation function of the fields at the two slits and it shows us the degree of spatial coherence of the light source. The increase of the inducing laser intensity makes the light source increasingly coherent in the spatial sense, until it behaves approximately as a laser beam, spatially coherent.

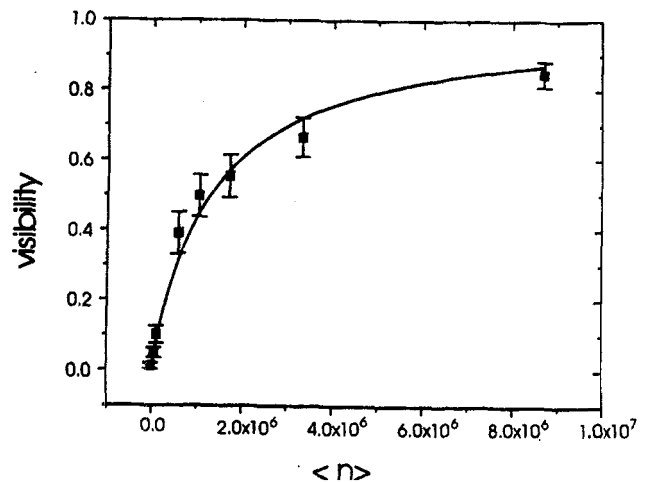


Figure 22. Experimental results (circle) and theory (line) for the Young's fringes visibilities as a function of the mean photon number ($\langle n \rangle$) of the inducing laser.

A change of field statistics, from thermal-like to laser-like, is implied by these results, as the transition from spontaneous to stimulated regime occurs.

It was then demonstrated that the spatial coherence in the signal beam can be controlled by means of its conjugated pair.

C. Temporal Coherence Properties of Stimulated Down-conversion

The temporal coherence properties of the stimulated parametric down-conversion process were also investigated experimentally. In this process we obtain a light beam which is a superposition of spontaneous and stimulated emission light.

In the stimulated parametric down-conversion process, an auxiliary laser is used to stimulate emission in one conjugated pair, signal and idler, of the down-converted light. Aligning the auxiliary laser with the idler beam direction, a signal beam is also stimulated. However, as the spontaneous emission process is still present, the resulting signal light beam is a superposition of spontaneous and stimulated emission light. The intensity of the spontaneous emission light depends on the pump laser intensity and on the down-conversion efficiency of the nonlinear crystal. On the other hand, the intensity of the stimulated emission light depends on the coupling between auxiliary laser field modes and down-conversion modes. Thus, for a fixed pump intensity, we can control the intensity ratio between stimulated and spontaneous emission light fields varying the auxiliary laser intensity.

The concepts of coherence in stimulated emission processes are important, for example, to signal amplification in optical fibers. In that case a weak coherent signal is amplified by stimulated emission, but corrupted by the noise from spontaneous emission always present. "Seeding" an Optical Parametric Oscillator (OPO) is another application of stimulated down-conversion to obtain narrow bandwidth lines.

The first order time coherence properties of the spontaneous emitted light depends on the spontaneous parametric down-conversion process and those of the stimulated emission light are dependent on the pump and auxiliary lasers properties. In Ref. [43], the spatial coherence properties of the signal beam produced in the stimulated down-conversion were studied. It was shown that the spatial degree of coherence is dependent on the intensity ratio between the stimulated emission

light, considered coherent, and the spontaneous emission light, considered incoherent.

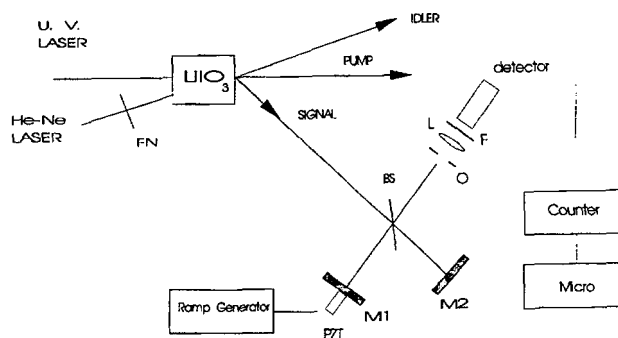


Figure 23. Outline of the experimental setup. The pump laser wavelength is 351.1 nm, the auxiliary laser wavelength is 632.8 nm, the signal beam central wavelength is 788.7 nm, the idler beam central wavelength is 632.8 nm, M1 and M2 are mirrors, P is a pinhole, I is lens, F is an optical filter, PCM is a photon counting module, BS is a beam-splitter, and PZT is a piezoelectric transducer.

In this section, the longitudinal, or temporal, coherence properties of the stimulated down-conversion is shown. Using a Michelson interferometer, the degree of coherence of this light beam as a function of the intensity ratio between the stimulated and spontaneous emission light fields was obtained. Varying the arms length of the interferometer, the degree of coherence as a function of the path difference was measured. (See Fig. 23).

The auxiliary laser is a He-Ne laser with wavelength $\lambda_a = 632.8$ nm. It is aligned with the idler beam, in order to stimulate its emission. The signal beam is then indirectly stimulated and directed to a Michelson interferometer. The mirrors of the interferometer are mounted on translation stages that allow a variation in their positions of about 4 cm with a $10 \mu\text{m}$ resolution. The position of one of these mirrors can be finely displaced by a piezoelectric transducer (PZT). This provides a way to vary the phase of the light reflected by the mirror.

The light emerging from the interferometer passes through a 0.8 mm diameter pinhole and is focused by a 15 cm focal lens to an avalanche diode detector. The auxiliary laser intensity is attenuated by neutral filters before the crystal, to vary the intensity ratio between spontaneous and stimulated emission fields.

In this experiment, the time coherence function $G(\tau)/G(0)$, or degree of temporal coherence, was mea-

sured for the polarized down-converted light field

$$\mu(\tau) = \frac{G(\tau)}{G(0)} = \frac{\langle \hat{E}^-(t - \tau_s) \hat{E}^+(t - \tau_s + \tau) \rangle}{\langle \hat{E}^-(t - \tau_s) \hat{E}^+(t - \tau_s) \rangle}, \quad (109)$$

where $\hat{E}(t)$ is the electric field operator of the light in time t after the pump laser is turned on, τ_s is the

time corresponding to the propagation of the signal field from the crystal to the interferometer, and τ is the time difference between fields traveling in different arms of the interferometer. To calculate the above correlation functions, we will follow the quantum multimode treatment already presented. The state of the field produced in the stimulated down-conversion is given by

$$\begin{aligned} |\psi(t)\rangle = & \{ |v_i(\omega_i)\rangle_i | \psi_{vac} \rangle_s + \\ & + \eta \frac{(\delta\omega)^{\frac{3}{2}}}{(2\pi)^{\frac{1}{2}}} \sum_{\omega_i} \sum_{\omega_s} \sum_{\omega_p} \phi(\omega_i, \omega_s; \omega_p) \frac{\sin(\omega_i + \omega_s - \omega_p)t_1/2}{(\omega_i + \omega_s - \omega_p)/2} \times \\ & \times e^{i(\omega_i + \omega_s - \omega_p)(t - t_1/2)} v_p(\omega_p) \hat{a}_i^\dagger(\omega_i) | \{v_i(\omega_i)\}_i | \omega_s \rangle_s, \end{aligned} \quad (110)$$

where v_i is the auxiliary laser coherent amplitude, $|\eta|^2$ is the down-conversion efficiency, ϕ is the spectral function for the down-conversion process, t_1 is the interaction time and \hat{a}_i^\dagger is the creation operator for the idler field.

The summations over ω'_i and ω'_p are easily performed, giving

$$\begin{aligned} G(\tau) = |\eta|^2 (\delta\omega)^2 \sum_{\omega_p} |v_p(\omega_p)|^2 e^{-i\omega_p\tau} \left[\sum_{\omega_i} |\phi(\omega_i, \omega_{p0} - \omega_i; \omega_{p0})|^2 e^{i\omega_i\tau} + \right. \\ \left. + \sum_{\omega_i} |\phi(\omega_i, \omega_{p0} - \omega_i; \omega_{p0})|^2 |v_i(\omega_i)|^2 e^{i\omega_i\tau} \right]. \end{aligned} \quad (111)$$

The coherence functions for the pump field, spontaneous emission field, and auxiliary laser field, can be defined as

$$G_p(\tau) = \frac{\delta\omega}{2\pi} \sum_{\omega} |v_p(\omega)|^2 e^{-i\omega\tau}; \quad (112)$$

$$G_{sp}(\tau) = 2\pi\delta\omega \sum_{\omega} |\phi(\omega, \omega_{p0} - \omega; \omega_{p0})|^2 e^{-i\omega\tau}; \quad (113)$$

$$G_{aux}(\tau) = \frac{\delta\omega}{2\pi} \sum_{\omega} |v_i(\omega)|^2 e^{-i\omega\tau}, \quad (114)$$

where $G_p(\tau) = G_p(-\tau)$ is the coherence function for the pump field, $G_{sp}(\tau)$ is the coherence function for the spontaneous down-conversion^[1], and $G_{aux}(\tau)$ is the coherence function for the auxiliary laser field. Considering that the spectral function ϕ is much broader than the auxiliary laser bandwidth, a final form for $G(\tau)$ is obtained^[43] as

$$G(\tau) = |\eta|^2 G_p(\tau) [G_{sp}^*(\tau) + (2\pi)^2 |\phi(\omega_{i0}, \omega_{p0} - \omega_{i0}; \omega_{p0})|^2 G_{aux}^*(\tau)], \quad (115)$$

where ω_{i0} is the central frequency of the idler beam.

The normalization of the above equation leads to

$$\mu(\tau) = \frac{G(\tau)}{G(0)} = \frac{G_p(\tau) [G_{sp}^*(\tau) + (2\pi)^2 |\phi(\omega_{i0}, \omega_{p0} - \omega_{i0}; \omega_{p0})|^2 G_{aux}^*(\tau)]}{G_p(0) [G_{sp}^*(0) + (2\pi)^2 |\phi(\omega_{i0}, \omega_{p0} - \omega_{i0}; \omega_{p0})|^2 G_{aux}^*(0)]} \quad (116)$$

or

$$\mu(\tau) = \mu_p(\tau) \frac{\mu_{sp}^*(\tau) + \mu_{aux}^*(\tau) \mathcal{N}}{1 + \mathcal{N}}, \tag{117}$$

where $\mu_p(\tau) = G_p(\tau)/G_p(0)$, $\mu_{sp}(\tau) = G_{sp}(\tau)/G_{sp}(0)$, $\mu_{aux}(\tau) = G_{aux}(\tau)/G_{aux}(0)$, $\mathcal{N} = (2\pi)^2 |\phi(\omega_{i0}, \omega_{p0}; \omega_{p0})|^2 G_{st}(0)$. $G_{sp}(0) = 1$ defines the normalization of the spectral function ϕ . Whenever $\mu_{sp} \ll \mu_{aux}$, to a good approximation a simple and very practical formula is obtained as

$$|\mu(\tau)| \approx |\mu_p(\tau)| \frac{|\mu_{aux}(\tau)| \mathcal{N}}{1 + \mathcal{N}}. \tag{118}$$

Within this simplification, the phases associated with the coherence functions are not necessary to the analysis of the experimental results. Some results will be presented, according to this simplified formula.

The Michelson interferometer provides a way to measure the coherence function $\mu(\tau)$. To each relative position of the mirrors M1 and M2 in Fig. 23, corresponds a time difference τ between the fields through the two arms of the interferometer. At given positions of these mirrors, a PZT scan shows the interference patterns. To obtain their visibilities $|\mu(\tau)|$, these patterns are fitted to the function^[44]

$$\mathbf{I} = 2I_0[1 + |\mu(\tau)| \cos(\omega\tau + \delta)], \tag{119}$$

where I_0 and δ are constants.

Fig. 24 shows the experimental curves of $\mu(\tau)$ as a function of r , for some values of \mathcal{N} . The values of \mathcal{N} are given by the signal count rate I_{sp} , with the auxiliary laser off, and the signal count rate I_{tot} , with the auxiliary laser on, since $\mathcal{N} \equiv I_{stim}/I_{sp} = (I_{tot} - I_{sp})/I_{sp}$. This relationship is consistent with the definition of \mathcal{N} ; it can be shown that $I_{tot} = |\eta|^2 \langle I_p \rangle (1 + \mathcal{N})$ and $\mathbf{I}_{\cdot} = |\eta|^2 \langle I_p \rangle$. These data were fitted by gaussians and the coherence length of the light field is given by their widths. The gaussian shape for $\mu(\tau)$ is defined by the shape of the coherence functions $\mu_p(\tau)$ of the pump laser and $\mu_{aux}(\tau)$ of the auxiliary laser.

The spectral density of a laser, and its temporal coherence function, which are Fourier transform counterparts, depends on three main line-broadening processes^[45]. The most important one, is the Doppler broadening, which is gaussian and has a FWHM of ~ 1.7 GHz.

The measurements show that the coherence length is independent of \mathcal{N} , for $\mathcal{N} \neq 0$. The optical filter and the pinhole placed in front of the detector determine the coherence length l_{sp} of the spontaneous emission light. In this case $l_{sp} < 10 \mu\text{m}$. For the measurements shown in Fig. 24, the separation between data points is of about 1 cm so that there is no resolution for ob-

serving the effects of the spontaneous emission light in the coherence length of the signal beam. The observed coherence length in Fig. 24 is due only to the stimulated emission light. It is defined by Eq. (117) with $\mu_{sp} = 0$, and given by the product $\mu_p(\tau) \times \mu_{aux}(\tau)$. The coherence length of the pump laser, measured with a Michelson interferometer, is $l_p = 2.8 \pm 0.2$ cm, and the coherence length of the auxiliary laser, which was measured with a Fabry-Perot scanning interferometer, is $l_{aux} = 39 \pm 4$ cm. The mean coherence length extracted from Fig. 24 is $l_{signal} = 3.7 \pm 0.5$ cm. It is larger than the the FWHM, $l_{eff} = 2.8$ cm, of the product $\mu_p(\tau) \times \mu_{aux}(\tau)$. Despite of this difference, Eq. (117) shows why the field stimulated by a 39 cm coherence length laser has its coherence length close to the coherence length of the pump laser.

Now, maintaining the mirrors fixed in a way that $r \sim 0$ and vary \mathcal{N} , through the auxiliary laser intensity, the interference patterns seen in Fig. 25 are obtained. The plot of their visibilities $|\mu(\tau \sim 0)|$ as a function of \mathcal{N} is seen in Fig. 26. In this situation $\mu_{sp} \sim 0$, because the resolution of the translation stages of the interferometer mirrors is not enough to set $r = 0$ within the precision required to obtain $\mu_{sp} \neq 0$ values. When the coherent field is of the same order of magnitude as the incoherent one ($\mathcal{N} \sim 1$), the degree of coherence decreases with the law given by Eq. 117. The theory fits well the experimental points when an upper bound for μ_{st} of Eq. (117) is used; the maximum visibility obtained experimentally is $|\mu(0)| = 0.9$. In principle, this parameter should be one, but some experimental limitations as dark noise background, finite detection area, and small differences on the reflection and transmission rates for the beam-splitter impose a maximum visibility smaller than one.

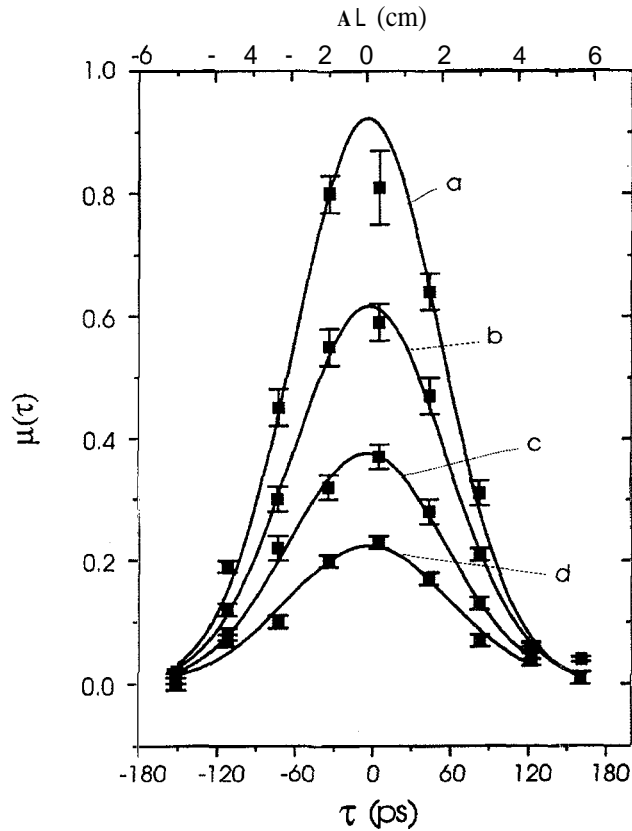


Figure 24. Modulus of the time coherence functions for stimulated down-conversion. The squares represent the experimental points and full lines are fittings to gaussians. Their FWHM are a) $w_a = 3.7 \pm 0.1$ cm for $\mathcal{N} = 15.5$, b) $w_b = 3.6 \pm 0.1$ cm for $\mathcal{N} = 1.81$, c) $w_c = 3.7 \pm 0.1$ cm for $\mathcal{N} = 0.68$, d) $w_d = 3.8 \pm 0.5$ cm for $\mathcal{N} = 0.37$.

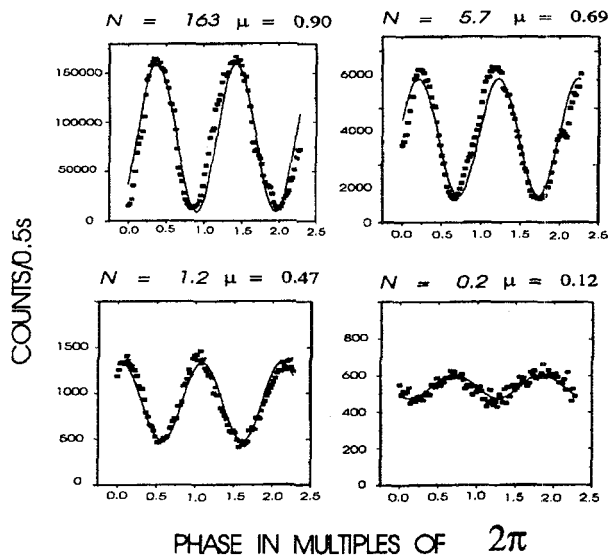


Figure 25. Interference patterns for $r \sim 0$ varying \mathcal{N} , and fittings.

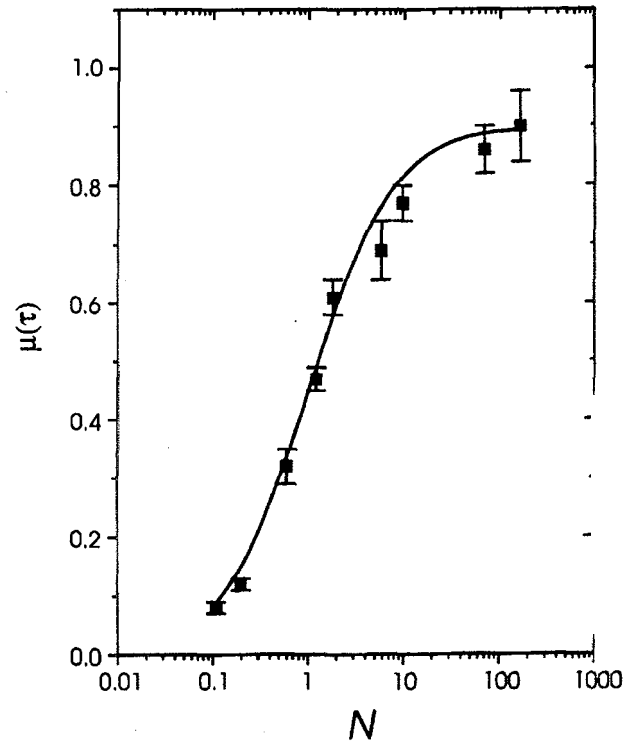


Figure 26. Plot of $|\mu(\tau \sim 0)|$ as a function of \mathcal{N} . Squares represent experimental points and full line is the theory with $\mu_{sp} = 0$ and $\mu_{aux} \times \mu_p = 0.9$.

The time coherence function for the light field generated in the stimulated down-conversion process was then obtained measuring the visibilities of the interference fringes obtained by passing this light through a Michelson interferometer, and varying the path difference defined by the positions of the interferometer mirrors. These measurements were performed for different intensity ratios between stimulated and spontaneous emission light.

The theory shows the dependence between the coherence properties of all fields involved in the stimulated down-conversion process, including the pump field. The experimental results are in agreement with the theory and show that the degree of coherence is affected by the presence of the spontaneous emission light when it is of the same magnitude as the stimulated emission light. However, the coherence length is due only to the stimulated emission light, even for small values of \mathcal{N} . This occurs because the detection scheme defines a very small coherence length for the spontaneous emission light, compared with the resolution of the interferometer. The results also show that the coherence length of the stimulated emission light depends on the overlap of the pump and auxiliary laser

coherence lengths.

VII. Beam-splitters, cavities and some applications

The quantum of energy of a single mode of the electromagnetic field, or photon, has been frequently thought as a localized fuzzy ball or just as a definition of the unit of light energy. However, strictly speaking, a single mode of an electromagnetic field is defined spatially within the whole universe accessible to this field. This universe can be, for example, a closed cavity or an open one, where in this last case the photon universe also includes the outside of the cavity accessible to the field. A photon can then be detected anywhere where the field is present.

The calculation of field modes for complex situations as an open cavity or in many other practical cases is a formidable challenge. Alternate methods or simplifications have been developed to deal with these situations. Usually, a light mode is treated, for example, before or after a beam-splitter or a pinhole, as a different mode. The practical success of these methods is what reinforces this broadly usage.

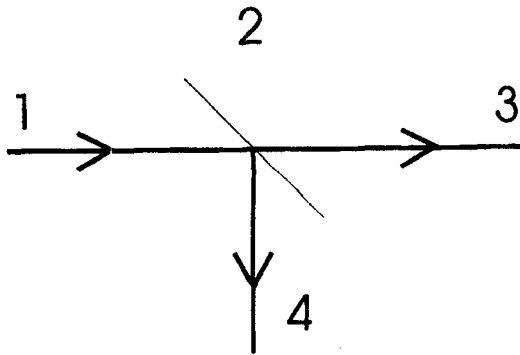


Figure 27. A beam splitter splits a light input from side "1", to outputs in sides "3" and "4". In side "2", $\langle n_2 \rangle = 0$.

Within this view, beam-splitters have been explored recently as "two-port" devices (See Fig. 27) where input and output "modes" are defined. In this picture, four distinct regions, 1, 2, 3 and 4, are considered. Light comes from site 1 and is distributed to sides 3 and 4.

Energy conservation implies that $E_1 = E_3 + E_4$. Consider, for example, E_1 written as $E_1 = \hbar\omega_1 (\langle n_1 \rangle + \frac{1}{2})$. In average, one photon may be detected in either side with a probability equal to one

half for a 50% beam-splitter. However, just considering the vacuum energies present in sides 1, 3 and 4 gives $(\hbar\omega/2)_1 = (\hbar\omega/2)_3 + (\hbar\omega/2)_4$, indicating some missing term. The vacuum energy balance is established by addition of a vacuum mode input in side 2, giving $(\hbar\omega/2)_1 + (\hbar\omega/2)_2 = (\hbar\omega/2)_3 + (\hbar\omega/2)_4$. The final image is then set according to Fig. 28, where \hat{a}_i are annihilation operators for input modes and \hat{b}_i operators for output modes. \hat{a}_2 , for example, could be the vacuum input necessary to the energy balance from side "2". Then it follows that

$$\begin{pmatrix} \hat{b}_1 \\ \hat{b}_2 \end{pmatrix} = \begin{pmatrix} s_{11} & s_{12} \\ s_{21} & s_{22} \end{pmatrix} \begin{pmatrix} \hat{a}_1 \\ \hat{a}_2 \end{pmatrix}. \quad (120)$$

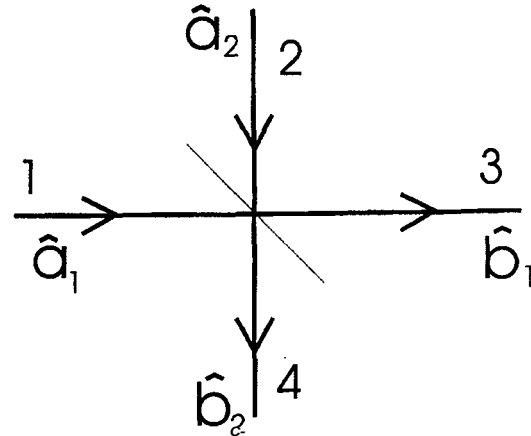


Figure 28. Light input comes from sides "1" and "2", where "2" has just vacuum energy.

Preservation of $[\hat{a}_i, \hat{a}_i^\dagger] = [\hat{b}_i, \hat{b}_i^\dagger] = 1$ in both sides of the beam-splitter leads to $|s_{11}|^2 + |s_{12}|^2 = 1$, $|s_{21}|^2 + |s_{22}|^2 = 1$ and $s_{11}s_{21}^* + s_{12}s_{22}^* = 0$.

Writing $s_{ij} = |s_{ij}|e^{i\phi_{ij}}$, the above conditions give $|s_{11}||s_{21}| = |s_{12}||s_{22}|$ and $\phi_{11} - \phi_{12} = \phi_{21} - \phi_{22} \pm \pi$. The $|s_{ij}|$ can be identified with the photon transmissivity t and photon reflectivity r , with $|t|^2 + |r|^2 = 1$ and $tr^* + rt^* = 0$. In this way, one obtains

$$\begin{pmatrix} \hat{b}_1 \\ \hat{b}_2 \end{pmatrix} = \begin{pmatrix} t & r \\ r & t \end{pmatrix} \begin{pmatrix} \hat{a}_1 \\ \hat{a}_2 \end{pmatrix}, \quad (121)$$

where t and r are scattering amplitude probabilities for the photon.

A lossless "etalon" or cavity can be treated along the same ideas. In a symmetric configuration, see Fig. 29, each interface is treated as the single beam-splitter and the medium introduces a phase shift δ_n as the field

propagates from one side to the other in the cavity. The procedure developed above is applied to each surface (t, r) in I and II, and the phase δ_n connects operators from side I to side II²⁰, resulting in

$$\begin{pmatrix} \hat{a}_t \\ \hat{a}_r \end{pmatrix} = \begin{pmatrix} \mu & \nu \\ \nu & \mu \end{pmatrix} \begin{pmatrix} \hat{a}_i \\ \hat{a}_v \end{pmatrix}, \quad (122)$$

where

$$\mu = \frac{t^2 e^{i\delta_n}}{1 - r^2 e^{2i\delta_n}} \text{ and } \nu = \frac{r + r(t^2 - r^2) e^{2i\delta_n}}{1 - r^2 e^{2i\delta_n}}, \quad (123)$$

with $|\mu|^2 + |\nu|^2 = 1$ and $\mu\nu^* + \nu\mu^* = 0$.

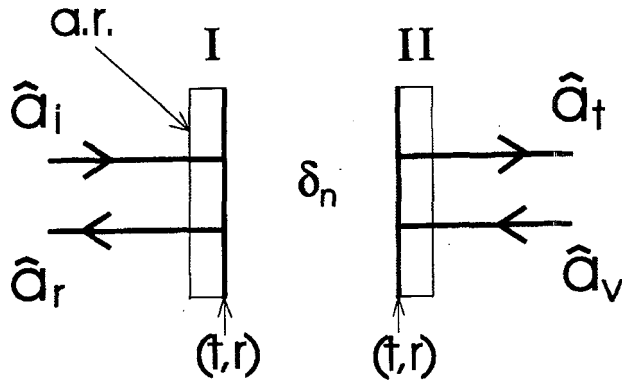


Figure 29. A simple symmetric cavity or etalon, with two inputs and two outputs.

Transmission probabilities of passive, active cavities and beam-splitters.

For an incoming beam with a photon distribution probability function $p(n)$ one could ask what is the probability distribution $p(n_t)$ of the beam after the splitting element. Consider an incoming beam described as a pure state $|\psi\rangle$, in the number basis $|n\rangle$

$$|\psi\rangle = \sum_{n=0}^{\infty} c_n |n\rangle = \sum_{n=0}^{\infty} c_n \frac{(\hat{a}^\dagger)^n}{\sqrt{n!}} |0\rangle. \quad (124)$$

From the last section one can see that $\hat{a}^\dagger = \nu\hat{a}_r^\dagger + \mu\hat{a}_t^\dagger$, where \hat{a}_r and \hat{a}_t are annihilation operators for reflected and transmitted fields, respectively. A simple binomial expansion gives²¹

$$(\hat{a}^\dagger)^n = (\nu\hat{a}_r^\dagger + \mu\hat{a}_t^\dagger)^n = \sum_{k=0}^n \frac{n!}{k!(n-k)!} (\nu\hat{a}_r^\dagger)^k (\mu\hat{a}_t^\dagger)^{n-k} \quad (125)$$

and, consequently,

$$|n\rangle = \sum_{k=0}^n \sqrt{\frac{n!}{k!(n-k)!}} \nu^k \mu^{n-k} |k_{(r)}, (n-k)_{(t)}\rangle. \quad (126)$$

The probability amplitude to find n , reflected photons and m_t transmitted ones within the "incoming" state is

$$(n, m_t | \psi) = \sum_{k=0}^n c_n \sqrt{\frac{n!}{k!(n-k)!}} \nu^k \mu^{n-k}, \quad (127)$$

so that

$$p(n_r, m_t; n) = p(n) \frac{n!}{n_r! m_t!} R^{n_r} T^{m_t}, \quad (128)$$

where $R = |\nu|^2$ and $T = |\mu|^2$, the reflectance and transmittance of the cavity. Summing up on all possible values of n , the probability to obtain m_t transmitted photons is

$$p(m_t) = \sum_{n \geq m_t}^{\infty} p(n) \frac{n!}{(n - m_t)! m_t!} R^{n - m_t} T^{m_t}. \quad (129)$$

A Poissonian input $p(n) = e^{-\langle n \rangle} \langle n \rangle^n / (n!)$ gives the output $p(m_t) = e^{-\langle T \rangle} (\langle T \rangle)^{m_t} / (m_t!)$, still a Poissonian output, with variance $\sigma^2 = \langle T \rangle$. Similarly, a Bose-Einstein input $p(n) = \langle n \rangle^n / (1 + \langle n \rangle)^{n+1}$ gives the output $p(m_t) = (\langle T \rangle)^{m_t} (1 + \langle T \rangle)^{m_t+1}$, a Bose-Einstein output with variance $\sigma^2 = \langle T \rangle [1 + \langle T \rangle]$. In these cases, the basic statistics is not changed.

However, for a non-classical field as a number state, with $p(n) = \delta(n - n_0)$, the transmitted distribution is the Binomial distribution $p(m_t) = (n_0! / m_t! (n_0 - m_t!)) T^{m_t} (1 - T)^{n_0 - m_t}$, with variance $\sigma^2 = n_0 T (1 - T)$. It is then seen that a so called *passive* beam-splitter (T and R are constants) randomizes the transmitted beam. This is very important when dealing with non-classical fields, because splitting optical elements interferes dramatically with a propagating beam.

One could question whether it is possible to have an active beam-splitter, with T and R variables, such that the transmitted beam could have a specified variance. This is the idea behind a dynamic cavity to produce sub-Poissonian fields described in Refs. [46,47].

²⁰ For example, $\hat{c}_1 = \hat{b}_1 e^{i\delta_n}$, etc.
²¹ In this case, there is no need to order the operators because they commute: The photons are distinguishable, because they are in different sides of the cavity (or beam splitter).

In Reference [46] a Fabry-Perot cavity is “filled” with a highly nonlinear medium such as a semiconductor multiple quantum well and conjugated down-converted beams are incident on the system. One of the beams, resonant with the excitonic energy, creates excitons producing a variation of the refractive index of the medium. This index variation is felt by the conjugated beam and, through a judicious choice of the MQW size and beam average intensity, an automatic modulation of the transmissivity of the second beam is produced. A final result is that the cavity could produce a sub-Poissonian beam at the output. This is a proposal to an all-optical-switch to generate non-classical fields.

At this point, it is interesting to remember the Q parameter introduced by Mandel to classify electromagnetic fields. For a single mode, this parameter can be written as

$$Q \equiv \frac{\langle \hat{a}^\dagger \hat{a}^\dagger \hat{a} \hat{a} \rangle}{\langle \hat{a}^\dagger \hat{a} \rangle^2} = \frac{\langle \Delta \hat{n}^2 \rangle - (E)}{\langle \hat{n} \rangle} \quad (130)$$

This parameter has value $Q = 0$ for Poissonian fields, $Q > 1$ for a super-Poissonian field and $Q < 1$ for the sub-Poissonian cases.

It is straightforward to show that, in a beam-splitter, Mandel’s parameter Q is *conserved*^[48]: If Q_i is the parameter associated to the incident field and Q_t and Q_r are the parameters connected with the transmitted and reflected fields, respectively, then

$$Q_i = Q_t + Q_r \quad (131)$$

In particular, if the *optical switch* described above^[46] generates a sub-Poissonian field in the transmitted field, then the reflected beam would show a super-Poissonian statistics, according to Eq. (131).

A beam splitter (BS) has also been used to create *two-photon* states, utilizing the PDC by superposition of a degenerate signal and idler pair on a beam splitter. With a careful matching of the beam paths to the BS, one can show (see Ref. [1]) that the two-photon state is created due to a quantum interference effect that forbids the appearance of single photons in either output side of the BS - two photons, instead, may appear in either side of the BS output. This special state has found interesting applications as, for example, to study wavepacket propagation through thin optical barriers. This study has revealed “superluminal” propagation^[49]

through the barrier. These apparent $v > c$ velocities are quite probably due to wavepacket dispersion effects within the barrier: One is lead to the problem of how to assign group velocity values to distorted wavepackets.

VIII. Conclusions

After this browsing over a few experiments utilizing PDC - exploring the second order nonlinearity $\chi^{(2)}$ in condensed matter - in crystals, particularly, a glimpse is obtained of the richness of this remarkable phenomenon. Recent studies have also explored the potentiality of organic and polymer materials as source for strong $\chi^{(2)}$ materials^[50].

It is stressed that fundamental questions can be studied even with *weak* beams from the downconversion process, in a diversion of the usual non-linear up-conversion studies where high intensities are involved. Of course, Quantum Mechanics is the appropriated realm to these studies with very low number of photons. Problems connected with longitudinal and transverse coherence properties were shown, including fundamental questions as the cause that imposes the coherence constraints between the two crystals in the “induced coherence without stimulated emission” or, the need for a full understanding of the concept of conjugated images (or “ghost” images) in the downconverted light field. Signal “teleportation”^[11] is also an adequate subject to explore the non-locality properties of the twin-beams of the PDC.

Practical applications usually follow basic advances in science. Currently, expensive U.V. and blue-violet lasers have been used to produce PDCL; one should expect that improvements in diode lasers can bring low cost accessible pump sources to the blue-violet range and that ideas now being explored in research laboratories may turn out commercially exploitable.

A very active research field involves the utilization of downconversion luminescence from crystals placed inside resonant optical cavities (Optical Parametric Oscillators - OPO). A broad interest then exists, from fundamental studies^[10,51] and applications ranging from spectroscopic studies with the squeezed fields produced by the OPO’s or the need to obtain wide tunable light sources. OPO cavities, designed for specific wavelengths produces oscillations in CW or pulsed regimes. Commercial OPO’s are now starting to appear, due to

better nonlinear crystals. A growing market signals a way to go.

In conclusion, it can be said that research on PDC reaches fundamental questions and shows promising application potentialities. University research can certainly profit from this fertile ground of research that also gives to graduate students these two perspectives – basic research and applied physics – so precious to a modern society.

Acknowledgements

Thanks are due to Prof. A. S. T. Pires, Drs. S. Pádua and P. H. Souto Ribeiro for a critical reading of the manuscript. This work was supported by the Brazilian research funding agencies CNPq, FINEP, and FAPEMIG.

References

1. L. J. Wang, X. Y. Zou, L. Mandel, Phys. Rev. A 44, 4614 (1991); X. Y. Zou, L. J. Wang, L. Mandel, Phys. Rev. Lett. 67, 318 (1991); Z. Y. Ou, L. J. Wang, L. Mandel, Phys. Rev. A 40, 1428 (1989); C. K. Hong, L. Mandel, Phys. Rev. Lett. 56, 58 (1986).
2. R. Andrews, E. R. Pike, and S. Sarkar, Phys. Rev. A 50, 2615 (1994).
3. D. C. Burham, D. L. Weinberg, Phys. Rev. Lett. 25, 84 (1970); W. H. Louisell, A. Yariv, A. E. Siegman, Phys. Rev. 124, 1646 (1961); D. Magde, H. Mahr, Phys. Rev. 171, 393 (1968); G. T. Giallorenzi, C. L. Tang, Phys. Rev. 166, 225 (1968); B. Ya. Zel'dovich, D. N. Klyshko, Sov. Phys. JETP Lett., 9, 40 (1969).
4. D. Eimerl, L. Davis, and S. Velsko, J. Appl. Phys. 62, 1968 (1987).
5. J. Q. Yao, T. S. Fahlen, J. Appl. Phys. 55, 65 (1984).
6. J. Toll, Phys. Rev. 104, 1760 (1956).
7. J. D. Jackson, Classical Electrodynamics, 2nd edition (Wiley, N.Y. 1975).
8. See, for example, D. F. Walls, Nature 306, 141 (1983).
9. R. E. Slucher, L. W. Hollberg, B. Yurke, J. C. Mertz, J. F. Velley, Phys. Rev. Lett. 55, 2409 (1985).
10. A. Heidmann, R. J. Horowicz, S. Reynaud, E. Giacobino, and C. Fabre, Phys. Rev. Lett. 59, 2555 (1987).
11. C. H. Bennett, S. J. Wiesner, Phys. Rev. Lett. 69, 2881 (1992); S. Popescu, Phys. Rev. Lett. 72, 797 (1994).
12. J. S. Bell, Physics 1, 195 (1965); L. Hardy, Phys. Lett. A 161, 21 (1991).
13. P. G. Kwiat, P. H. Eberhard, A. M. Steinberg, and R. Y. Chiao, Phys. Rev. A 49, 3209 (1994).
14. G. S. Agarwal, J. Opt. Soc. Am. B 5, 1940 (1988).
15. N. Zagury, Estatística de Fótons, "Summer School Jorge André Swieca" (Brazilian Physical Society, 1986), pg. 3 and, ibidem G. A. Barbosa, pg.47.
16. R. J. Glauber, Phys. Rev. 130, 2529 (1963); Phys. Rev. 131, 2766 (1963).
17. J. T. Sakurai, Modern Quantum Mechanics, Edited by S. F. Tuan (Addison-Wesley, N.Y. 1985).
18. C. Heitor d'Ávila Fonseca (UFMG), private communication (1994).
19. A. S. Davydov, Quantum Mechanics (Pergamon Press, N.Y. 1968).
20. A. Garuccio, Annals of the New York Academy of Sciences 755, 633 (1995).
21. F. T. Arecclii, Ottica quantistica - Ed. by R. J. Glauber (Academic Press, N.Y. 1969).
22. C.H. Monken, G.A. Barbosa; Optical Commun. 99, 152 (1993).
23. L. Maialel, Opt. Lett. 16, 1882 (1991).
24. T. Grayson and G.A. Barbosa; Phys. Rev. A 49, 2948 (1994).
25. G. A. Barbosa, Phys. Rev. A 48, 4730 (1993).
26. M. Born, E. Wolf, Principles of Optics (Pergamon Press, New York, 1959) pg. 535; G. B. Parrent Jr., J. Opt. Soc. Soc. Am. 49, 787 (1959); P. H. Van Cittert, Physica 6, 1129 (1939); F. Zernike, Physica 5, 785 (1938).
27. X.Y. Zou, T. Grayson, G.A. Barbosa, and L. Mandel; Phys. Rev. A 47, 2293 (1993).
28. T. Grayson, J.R. Torgerson, and G.A. Barbosa; Phys. Rev A 49, 626 (1993).
29. M. V. Berry, Proc. R. Soc. London A 392, 45 (1984); Y. Aharnov, J. Anadam, Phys. Rev. Lett. 58, 1593 (1987).

30. S. Pancharatnam, Proc. Indian Acad. Sci. Sect. A 44, 247 (1956); R. Y. Chiao, Y. S. Wu, Phys. Rev. Lett. 57, 933 (1986); A. Tomita, R. Y. Chiao, Phys. Rev. Lett. 57, 937 (1986); P. G. Kwiat, R. Y. Chiao, Phys. Rev. Lett. 66, 588 (1991).
31. M. Born and E. Wolf, *Principles of Optics*, 6th ed. (Pergamon, N.Y., 1980); J. P. Mathieu, *Optics* (Pergamon, N.Y. 1975); M. G. Rousseau, J. P. Mathieu, *Problems in Optics* (Pergamon, N.Y., 1973).
32. B. Yurke, S. L. McCall, J. R. Klauder, Phys. Rev. A 33, 4033 (1986); R. Campos, B. Saleh, and M. Teich, Phys. Rev. A 40, 1371 (1989).
33. G. A. Barbosa, Phys. Rev. A 50, 3379 (1994).
34. K. J. McNeil, C. W. Gardiner, Phys. Rev. A 28, 1560 (1983); C. W. Gardiner, M. J. Collet, Phys. Rev. A 31, 3761 (1985); P. D. Drummond, C. W. Gardiner, J. Phys. A: Math. Gen. 13, 2353 (1980); A. S. Lane, M. D. Reid, D. F. Walls, Phys. Rev. A 38, 788 (1988).
35. C. W. Gardiner, *Handbook of Stochastic Methods* (Springer-Verlag, Berlin, 1990) 2nd edition.
36. T. J. Herzog, J. G. Rarity, H. Weinfurter, and A. Zeilinger, Phys. Rev. Lett. 72, 629 (1994).
37. M. Born and E. Wolf, *Principles of Optics*, 2nd ed. (Pergamon Press, New York, 1964), pp. 499-513.
38. P. H. S. Ribeiro, C. H. Monken, and G. A. Barbosa, Appl. Optics. 33, 352 (1994).
39. P. H. S. Ribeiro, S. Pádua, J. C. Machado da Silva, and G. A. Barbosa, Phys. Rev. A 49, 4176 (1994).
40. D. Greenberger, M. A. Horne, and A. Zeilinger, Phys. Today 49, 22 (1993).
41. J. Rehacek and J. Perina; 7th Rochester Conference on Coherence and Quantum Optics (1995).
42. Y. H. Shih, A. V. Sergienko, T. B. Pittman, D. V. Strekalov, and D. N. Klyshko; Annals New York Academy of Science, 121 (1994); D. V. Strekalov, A. V. Sergienko, D. N. Klyshko, and Y. H. Shih, Phys. Rev. Lett. 74, 3600 (1995).
43. P. H. Souto Ribeiro, S. Pádua, J. C. Machado da Silva, and G. A. Barbosa, Phys. Rev. A 51, 1631 (1995).
44. See for example B. E. A. Saleh and M. C. Teich, *Fundamentals of Photonics*, (Wiley, N.Y., 1991) p. 360.
45. See for example K. Thyagarajan and A. K. Ghatak, *Lasers Theory and Applications*, (Plenum, New York, 1981) p. 54.
46. G.A. Barbosa, C.H. Monken; Phys. Rev. Lett. 67, (1991) 3372.
47. C. Fabre, R. J. Horowicz; Opt. Comm. 107, 420 (1994).
48. J. Noh, private communication (University of Rochester, 1993).
49. R. Y. Chiao, International Quantum Electronics Conference, paper QThH3, pg. 202 (Optical Society of America, 1994); A. M. Steinberg, R. Y. Chiao, Phys. Rev. A 51, 3525 (1995).
50. A. Garito, R. F. Shih, and M. Wu, Phys. Today, (May 1994) pg. 51.
51. R. Vyas and S. Singh, Phys. Rev. Lett. 74, 2208 (1995); L. Wu, H. J. Kimble, J. L. Hall, and H. Wu, Phys. Rev. Lett. 57, 2562 (1986).